

**Removal of Cationic Dye Using a Magnetic Nanocomposite Based on
Poly(acrylic Acid) and Carboxylated Cellulose Nanocrystal**

by

RAJIB SAMADDER

STUDENT ID: 0416032708

MASTER OF SCIENCE IN CHEMISTRY



Department of Chemistry

BANGLADESH UNIVERSITY OF ENGINEERING AND TECHNOLOGY

2018

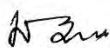
The thesis titled "Removal of Cationic Dye Using a Magnetic Nanocomposite Based on Poly(Acrylic Acid) and Carboxylated Cellulose Nanocrystal" submitted by Rajib Samadder, Roll No. 0416032708, Session: April 2016, has been accepted as satisfactory in partial fulfillment of the requirement for the degree of Master of Science in Chemistry on May 26, 2018.

BOARD OF EXAMINERS



1. Dr. Md. Shafiu Azam
Assistant Professor
Department of Chemistry
BUET, Dhaka

Chairman



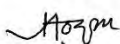
2. Dr. Md. Abdur Rashid.
Professor & Head
Department of Chemistry
BUET, Dhaka

Member
(Ex-officio)



3. Dr. Md. Shakhawat Hossain Firoz
Professor
Department of Chemistry
BUET, Dhaka

Member



4. Dr. Md. Anamul Hoque
Professor
Department of Chemistry
Jahangirnagar University
Savar, Dhaka-1342

Member
(External)

CANDIDATE'S DECLARATION

It is hereby declared that this thesis or any part of it has not been submitted elsewhere for the award of any degree or diploma.

Rajib Samadder

Dedicated to

My Beloved Family

&

Honorable supervisor

Table of Contents

List of Tables and Figures..... vi

List of Tables and Abbreviations of Technical Symbols and Terms viii

Acknowledgement x

Abstract xii

List of Tables and Figures

Figures

Figure 1.4.1. Schematic illustration of Coagulation process.....	05
Figure 1.5 Schematic illustration of adsorption process	07
Figure 1.7.2 Cross sectional representation of cellulose nanocrystal indicating the occurrence of the surface TEMPO-mediated oxidation of available hydroxyl groups	10
Figure 2.1 Schematic representation of carboxylated cellulose nanocrystals.....	26
Figure 3.1 Schematic representation of 3D crosslinker synthesis	32
Figure 3.2 Mechanism of TEMPO mediated oxidation (a) initial formation of oxidant from TEMPO radical and (b) catalytic cycle of TEMPO oxidation.....	33
Figure 3.3 Schematic representation of nanocomposie synthesis.....	34
Figure 3.4 FTIR spectra of Fe ₃ O ₄ , silica coated Fe ₃ O ₄ , aminated Fe ₃ O ₄ and Acrylated Fe ₃ O ₄	36
Figure 3.5 FTIR spectra of CNC, CCN and nanocomposite.....	37
Figure 3.6 Widescan spectra of aminated Fe ₃ O ₄ , acrylated Fe ₃ O ₄ and nanocomposite	38
Figure 3.7 High resolution of C1s spectra of aminated Fe ₃ O ₄ , acrylated Fe ₃ O ₄ and nanocomposite.....	40
Figure 3.8 High resolution of N1s spectra of aminated Fe ₃ O ₄ , acrylated Fe ₃ O ₄ and nanocomposite.....	41
Figure 3.9 FE-SEM image of magnetic iron oxide nanoparticle (Fe ₃ O ₄) (A) Resolution x 100,000 (B) Resolution x 150,000.....	41
Figure 3.10 FE-SEM image of silica coated Fe ₃ O ₄ (A) Resolution x 50,000 (B) Resolution x 100,000.....	42
Figure 3.11 FE-SEM image of acrylated Fe ₃ O ₄ (A) Resolution x 100,000 (B) Resolution x 150,000.....	43

Figure 3.12 FE-SEM image of CCN (A) Resolution x 50,000 (B)Resolution x 100,000.....	44
Figure 3.13 FE-SEM image of nanocomposite (A) Resolution x 100,000 (B) Resolution x 150,000.....	45
Figure 3.14 EDX spectra of (A) Fe ₃ O ₄ and (B) silica coated Fe ₃ O ₄	47
Figure 3.16 EDX spectra of (C) acrylated (Fe ₃ O ₄)	48
Figure 3.17 EDX spectra of (D) CCN and (E) nanocomposite.....	49
Figure 3.18 TGA curves of CCN, acrylated Fe ₃ O ₄ , composite without CCN and nanocomposite.....	50
Figure 3.19 Magnetic hysteresis loop of Fe ₃ O ₄ , Acrylated Fe ₃ O ₄ and PAA/Fe ₃ O ₄ /CCN (PAAMCCN) composite.....	52
Figure 3.20 Adsorption capacity q _t of MB on Acrylated Fe ₃ O ₄ and PAA/Fe ₃ O ₄ /CCN (PAAMCCN).....	53
Figure 3.21 Fitting the adsorption kinetics of MB on PAAM and PAAMCCN using the pseudo-first order kinetic model.....	54
Figure 3.22 Fitting the adsorption kinetics of MB on PAAM and PAAMCCN using the pseudo-second-order kinetic model.	55
Figure 3.23 Isotherms of the adsorption of MB on (a) PAAM and (b) PAAMCCN, with a contact time of 14 h.....	58
Figure 3.24 Adsorption capacity of MB on PAAM and PAAMCCN under different pH	59
Figure 3.25 Zeta potential of Acrylated Fe ₃ O ₄ and PAAMCCN.....	60

Tables

Table 3.1 Characteristic IR bands of CNC, CCN and nanocomposite.....	38
Table 3.2 Elemental composition of magnetic and cellulosic compound.....	46
Table 3 Parameters for the fitting of the adsorption of MB on PAAM and PAAMCCN using the pseudo-first-order and pseudo-second-order kinetic models..	56

List of Abbreviations of Technical Symbols and Terms

1. Carboxylated cellulose nanocrystal (CCN).
2. Acrylated Fe₃O₄ (3D)
3. Poly acrylic acid (AA)
4. Poly acrylic magnetic Fe₃O₄ (PAAM)
5. Poly acrylic magnetic Fe₃O₄ Carboxylated cellulose nanocrystal (PAAMCCN)
6. Nanoparticle (NP)

Acknowledgement

At the very beginning, I humbly acknowledge my deepest gratitude to the almighty, the most gracious, benevolent and merciful creator for his infinite mercy bestowed on me in carrying out the research work presented in the dissertation.

It is a great pleasure for me to acknowledge my deepest sense of gratitude, sincere, appreciation, heartfelt indebtedness and solemn regards to my reverend teacher and supervisor Dr. Md. Shafiul Azam, Assistant Professor, Department of Chemistry, Bangladesh University of Engineering and Technology (BUET), for his kind supervision, indispensable guidance, valuable and constructive suggestions, liberal help and continuous encouragement during the whole period. It is obvious that his attributive contribution and efforts have greatly shaped me into what I am today. In fact, I am quite lucky to be a part of his ambitious research team.

It is my great honor to convey my sincere gratitude to my respected teacher Professor Dr. Md. Abdur Rashid, honorable Head of the Department of Chemistry, BUET for giving me his wonderful support to move through the academic processes during this M.Sc. program. I would like to convey my deepest gratitude to Professor, Dr. Md. Rafique Ullah, Dr. Md. Shakhawat Hossain Firoz, Dr. Abu Bin Imran, Dr. Chanchal Kumar Roy, Anika Auni and Nahida Akter Department of Chemistry, BUET, for their valuable suggestions, appreciated comments, guidance and help during the research period. I am thankful to all other respected teachers of the Department of Chemistry, BUET, for their time to time support. I would also like to thank all of the officers and staffs of the Department of Chemistry, BUET for their continuous help during my study period.

I am highly thankful to Professor Dr. Hongbo Zeng, University of Alberta, Canada, for the characterization of our samples using X-ray Photoelectron Spectroscopy (XPS), Zeta Potential technique during my research.

I am highly grateful to all members of the board of examiners for their valuable suggestions and appreciated comments.

I would like to express my sincere gratitude to A. K. M. Atique Ullah, Scientific Officer Chemistry Division, Atomic Energy Centre, Bangladesh Atomic Energy Commission, Dhaka, Bangladesh for his generous help and kind support of materials characterization during the research period.

I am thankful to my dear colleagues and all the members of Azam Research Group for their friendly cooperation and lovely encouragement throughout my research period. Special thanks to Abinash Chandra Roy, Md. Ferdous, Md. Majharul Islam, Rubel Habib, Fatema Zerin Farhana, Al Mamun Rasel, Mosfeq Uddin(Nadeem), Bushra Upoma, Imon, Noman, Tarun, and Solaiman for their continuous help during the research.

I am also thankful to other fellows of Chemistry Materials Laboratory for their cooperation during the research period.

I am grateful to the authority of BUET and The World Academy of Sciences (TWAS) for providing financial support for this research work.

Finally, I would like to express my heartfelt indebtedness and profound gratitude to my beloved father, mother and all of my family members for their continuous inspiration and immeasurable sacrifices throughout the period of my study.

May, 2018

Rajib Samadder

Abstract

Dyes are broadly used in various industries like textile, paper and pulp, dyestuffs and plastics. Miscellaneous activities at the industries discharge wastewater with extensive amount of carcinogenic dyes, which cause various environmental and health problems. Nowadays, various technologies have been invented and applied for the removal of dyes from wastewater. Among these methods, adsorption has received much attention due to its high efficiency, simplicity and economic viability. Herein, we present a novel magnetic nanocomposite based on polyacrylic acid and carboxylated cellulose nanocrystal(CCN), for effective adsorption of cationic dyes and easy magnetic separation of the adsorbent nanocomposite from the wastewater after the adsorption process. The functionalization of Fe_3O_4 was performed by carrying out an in situ polymerization of acrylic acid, CCN and acrylic modified Fe_3O_4 , which will act as a crosslinker. The fabricated nanocomposites were characterized employing FTIR, XPS, FESEM, TGA, Zeta Potential and Magnetization. The magnetization (magnetization vs magnetic field) hysteresis of the nanocomposite confirmed the magnetic nature of the as-synthesized materials. The synthesized nanocomposite exhibited excellent adsorption for methylene blue and the kinetics data were fitted to pseudo-first-order and pseudo-second-order models to figure out the adsorption mechanism where, the resultant data support mostly to pseudo second order kinetic model. We also studied adsorption using Langmuir and Freundlich isotherm model where adsorption followed the Langmuir isotherm model. The effects of pH on the adsorption of dye were also investigated by monitoring the kinetics at variable pH. The pH dependent zeta potential was employed to describe the observed pH effects on the adsorption capacity.

Contents

CHAPTER 1: Introduction

1.1 General Remarks	02
1.2 Background.....	02
1.3 Reviews on Some Recent Works on Dyes	03
1.4 Literature review.....	04
1.4.1 Coagulation.....	05
1.4.2 photocatalysis	05
1.4.3 Filtration.....	06
1.5 Adsorption Principles	06
1.6 Types of adsorbent.....	07
1.6.1 Clay	08
1.6.2 Zeolite.....	08
1.6.3 Activated Carbon.....	08
1.7 Magnetic Adsorbent.....	09
1.7.1 Three dimensional crosslinker.....	09
1.7.2 Carboxylated Cellulose nanocrystals (CCN).....	10
1.7.3 Magnetically responsive polymer composite.....	11
1.8 Research Goal	12
References.	13

CHAPTER 2: Experimental

2.1 Chemical and reagents.....	23
2.2 Instruments.....	24
2.2 Synthesis of magnetic nanocomposite.....	25
2.3.1 Synthesis of acrylated magnetic iron oxide nanoparticles	25
2.3.1.1 Synthesis magnetic iron oxide nanoparticles (Fe_3O_4).....	25
2.3.1.2 Synthesis Silica Coated magnetic iron oxide nanoparticles.....	25
2.3.1.3 Synthesis Aminated magnetic iron oxide nanoparticles.....	25

2.3.1.4 Synthesis Acrylated magnetic iron oxide nanoparticles (3D).....	26
2.3.2 Synthesis of carboxylated cellulose nanocrystals (CCN).....	26
2.3.3 Synthesis of nanocomposite.....	27
2.4 Sample characterization.....	27
2.4.1 Fourier transform infrared analysis (FTIR).....	27
2.4.2 Field emission scanning electron microscopy (FE-SEM)	28
2.4.3 Energy dispersive x-ray (EDX) spectra.....	28
2.4.4 X-ray photoelectron spectroscopy (XPS)	28
2.4.5 Thermogravimetric analysis (TGA).....	29
2.4.6 Magnetic Property Analysis.....	29
2.4.7 Adsorption Experiments:.....	29
2.4.8 Zeta Potential	29
References.	30

Chapter 3: Results and Discussion

3.1 Synthesis of acrylated Fe ₃ O ₄ (3D) crosslinker.....	32
3.2 Synthesis of carboxylated cellulose nanocrystals (CCN).....	32
3.3 Synthesis of Nano Compositote	34
3.4 Functional group analysis using FTIR.....	35
3.5 X-ray photoelectron spectroscopy (XPS).....	38
3.5.1 High Resolution C1s Spectra.....	39
3.5.2 High Resolution N1s Spectra.....	41
3.6 Surface morphology study using field emission scanning electron microscope (FE-SEM).....	42
3.7 Energy dispersive x-ray (EDX) spectral analysis.....	46
3.8 Thermogravimetric analysis	50
3.9 Magnetic property analysis.....	51
3.10 Dye (Methylene blue) removal experiment.....	52
3.10.1 Adsorption Test	52
3.10.2 Pseudo-first order model.....	53
3.10.3 Pseudo-second order model.....	54

	3
3.10.4 Langmuir isotherm.....	56
3.10.5 Freundlich isotherm model	57
3.10.6 Effect of pH	58
3.10.7 Effect of pH on zeta potential.....	59
3.11 Conclusion.....	60
References.	61

CHAPTER 1

Introduction

1.1 General Remarks

Saving water to save the planet and to make the future of mankind safe is what we need now. With the growth of mankind, society, science, technology our world is

reaching to new high horizons but the cost which we are paying or will pay in near future is surely going to be too high. Among the consequences of this rapid growth is environmental disorder with a big pollution problem. Anthropogenic activities have caused a great harm to the quality of our lifeline, i.e. water. Because of fast depletion of the freshwater resources, there seems to be a crisis of the same. Water pollution is a global concern and, it is the high time that we realize the gravity of the situation. Removing pollutants from water is the crying need of the hour and developing a cost effective and environmentally safe method to achieve the same is a challenging task for chemical engineers. After all, it is the future of mankind, which is at stake.

A dye is a colored element that has an affinity to the substrate to which it is being applied. Dyes appear to be colored because they absorb some wavelengths of light more than others. Humans are estimated to use dyes for thousands of years and the earliest use of the colorant is believed to be by Neanderthal man about 1,80,000 years ago [5,13]. The year 1856 witnessed a historic discovery of first synthetic dye, Mauvine, by Perkin [14, 15]. In due course of time, these synthetic dyes gained great popularity and began to be synthesized on a large scale. In fact, it has reached to a level of annually, over 7.0×10^5 and nearly 1000 different types of dyes are produced worldwide [2].

1.2 Background

Now-a-days, a large amount of wastewater having color is generated by many industries like textile, leather, paper, printing, plastic and so on [1]. The presence of dye materials greatly influence the quality of water and the removal of this kind of pollutant is of prime importance. For their intricate chemical structures, dyes are difficult to manage with municipal waste treatment operations [2]. A little quantity of dye does cause high visibility and undesirability. Moreover, the color created by dyes in water makes it aesthetically unpleasant [1]. They can have acute or chronic effects on exposed organisms, which depend on the concentration of the dye and the exposed time [2]. In addition to that, many dyes are considered to be toxic and even carcinogenic [1,3,4].

Few decades earlier the dye selection, applications and uses were not given much importance. With the growing health concerns, it was in the 80s that people started paying much attention to the dye wastes [5]. An indication to the magnitude of this

problem can be inferred from the fact that two percent of dyes produced are directly discharged into aqueous effluents [6,7]. With the increased stringent laws on industrial discharge, it has become very important to treat this wastewater. Because of their detriment and large scale distribution in the ecological environment, their separation and determination has become one of the important studies of environmental analysis. Of prime importance is the need for clear information on the safety related properties of the colorants and the measure to be taken for lowering exposure. If all these elements are seriously considered, then the technical use of colorants and the handling involved might be possible without much health danger.

1.3 Reviews on Some Recent Works on Dyes

Different studies have been prosecution on the adsorption of different types of dyes from various adsorbents.

In 2015, the removal of methylene blue from the waste water using poly (acrylic acid) functionalize magnetic grapheme oxide nano composite(PAA/MGO) [8]. The adsorption of dye on PAA/MGO was investigated in batch process. The adsorption capacity of MB on adsorbent also investigate in different pH. The composite shows high adsorption rate, adsorption capacity, easy separation and good recyclability.

In 2012, the adsorption of acid blue 25, Cd^{2+} and Zn^{2+} on a physically activated bituminous carbon and a phosphoric activated carbon from wood was studied using single and binary (dye/metal) solutions[17]. It was found that the presence of Acid blue 25 (AB25) on dye–metal binary solutions enhanced the adsorption of Zn^{2+} and Cd^{2+} on bituminous and wood commercial ACs in a very similar way, in spite of the differences of the textural and surface chemistry properties of both carbons

In 2012, adsorption of acid dyes on SBA-3 ordered mesoporous silica, ethylenediamine functionalized SBA-3 (SBA-3/EDA), aminopropyl functionalized SBA-3 (SBA-3/APTES) and pentaethylene hexamine functionalized SBA-3 (SBA-3/PEHA) materials was studied [18]. The SBA-3/PEHA was found that it has the highest adsorption capacity for all acidic dyes. Batch studies were performed to study the effect of various experimental parameters such as chemical modification, contact time, initial concentration, adsorbent dose, agitation speed, solution pH and reaction temperature on the adsorption process. The Freundlich model was found to be fit with the equilibrium isotherm data.

In 2011, dye removal from colored textile wastewater using chitosan in binary system was studied [19]. Here, Direct Red 23 and Acid Green 25 were used as anionic dyes. The adsorption kinetics of dyes on chitosan followed the pseudo second order at different pH values. The experimental data were correlated reasonably well by Tempkin adsorption isotherm. It was concluded that the chitosan is an eco- friendly adsorbent for dye removal from low concentration of acidic colored textile wastewater.

In 2010, chemically modified sugarcane bagasse as a potentially low-cost biosorbent for the removal of methyl red was studied [20]. The kinetics of methyl red adsorption followed the pseudo first order kinetic expression and Langmuir isotherms model fit well. From the study, it was conjectured that sugarcane bagasse has a good ability to be used for small scale industries, which produces dyes as their effluent, after it was being pretreated with phosphoric acid.

.In 2010, the removal of reactive red 23, reactive blue 171, acid black 1 and acid blue 193 from aqueous solution using fly ash was studied [21]. The results indicate that adsorption was pH dependent, adsorption increased with the initial dye concentration; the reaction was spontaneous and exothermic in nature.

In 2010, the porous magnetic microspheres prepared with sulfonated microporous polydivinylbenzene as a template and their ability to remove cationic dyes was studied [22]. The consequence of the study show that the methyl violet and basic fuchsin can be successfully withdraw from the solution using the adsorbent and even the adsorbent is easily regenerated.

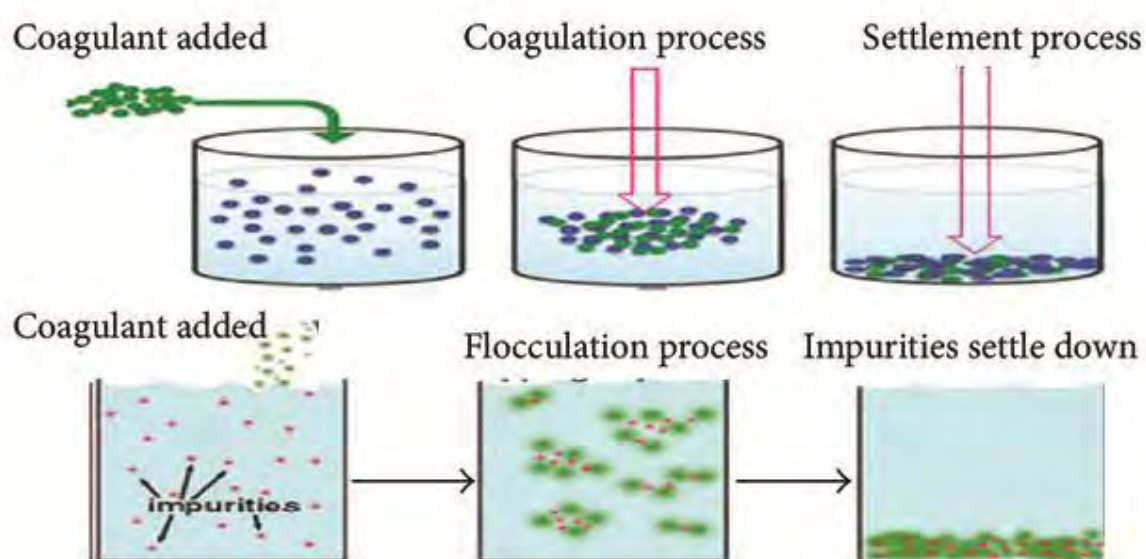
1.4 Literature review

Moreover, dyes are generally toxic to aquatic lives and cannot be easily degraded by microorganisms [27]. Therefore, economically viable techniques to efficiently remove dye contaminants from wastewater are highly desirable. Various technologies have been invented and applied for the removal of dyes from wastewater, including coagulation/flocculation [28], photocatalysis [29], ultrafiltration [30] and adsorption [31]. Among these methods, adsorption has received much attention due to its high efficiency, simplicity and economic viability [32,33].

1.4.1 Coagulation

CHAPTER 1 Coagulation is a easy wastewater treatment method. In this method the addition of chemicals to change the physical state of solution and suspended solids and facilitate their removal by sedimentation. For a long time the Coagulation method for treatment of dye-containing wastewater has been used as main method for its low capital cost [34, 35]. However, the generation of sludge and ineffective decolorization of some soluble dyes was the main limitation of this process [34, 36].

CHAPTER 2



CHAPTER 3 **Figure 1.4.1. Schematic illustration of Coagulation process.**

CHAPTER 4 1.4.2 photocatalysis

CHAPTER 5 Catalyst increases the rate of a chemical reaction without itself undergoing any permanent chemical change. Using catalytic agent, one can reduce the temperature of a chemical transformation, reduce reagent-based waste and increase the selectivity of a reaction that avoids the unwanted side reactions which leads to the green chemistry. There are some limitations in this method. The photocatalytic degradation mainly occurs on the surface of solute, Some catalytic agent show

minimized effect for application in water treatment. The poor affinity against organic pollutants (especially the hydrophobic organic pollutants), the adsorption of organic pollutants on catalytic agent surface is relatively low, resulting in slow photocatalytic degradation rates [37].

1.4.3 Filtration

CHAPTER 6 Filtration is the most common methods in the filtration technology. Filtration methods such as ultrafiltration, nanofiltration and reverse osmosis have been used for water reuse and the chemical recovery [38,39]. In the textile industry, these filtration methods can be used for both filtering and recycling of not only pigment rich wastewaters, but also mercerizing and bleaching wastewaters. The specific temperature and chemical composition of the wastewaters determines the type and porosity of the filter to be applied. Further, the utilization of membrane technology for dye removal from textile wastewater is very effective as reported by various researchers [40, 41]. However, the main drawbacks of membrane technology are the high cost, frequent membrane fouling, requirement of different pretreatments depending upon the type of influent wastewaters, and production of concentrated dye-bath which further needs proper treatment before its safe disposal to the environment [42, 43]. For membrane filtration, proper pretreatment units for removing suspended solid of the wastewaters are almost mandatory to increase the life time of the membranes. These make the process more expensive and thereby limit the application.

1.5 Adsorption Principles

Adsorption is a procedure, when a solute pile up on the surface of a solid or a liquid, create a molecular or atomic film. On the other hand the adsorption is the adhesion of atoms, ions, biomolecules or molecules of gas, liquid, or dissolved solids to a surface and this process creates a film of the adsorbate (the molecules or atoms being accumulated) on the surface of the adsorbent. It is a surface phenomenon and a consequence of surface energy. The atoms on the surface of the adsorbent are not wholly surrounded by other atoms and thus, can attract adsorbates. The nature of the

bonding confide on the details of the elements involved, but the adsorption process is generally classified as follows:

- (1) Physisorption: It is a type of adsorption in which the adsorbate adheres to the surface through Van der Waals (weak intermolecular) interactions.
- (2) Chemisorption: It is a type of adsorption whereby a molecule adheres to a surface through the formation of a chemical bond.

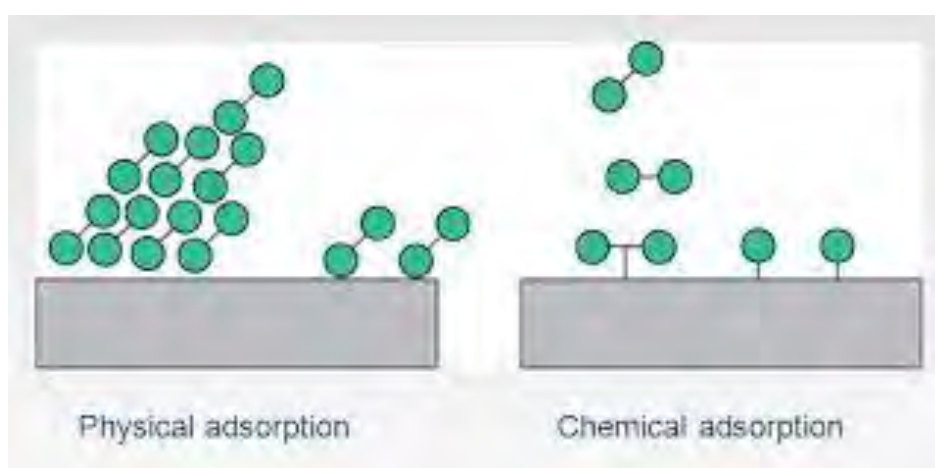


Figure. 1.5. Schematic illustration of adsorption process

Adsorption takes place primarily on the walls of the pores or at specific sites inside the particle. As the pores are generally small, the internal surface area is greater than the external area. Separation occurs because differences in molecular weight, shape or polarity cause some molecules to be held more strongly on the surface than others. In many cases, the adsorbate is held strong bond to allow complete removal of that component from the fluid [16].

1.6 Types of adsorbent

A variety of adsorbents such as clay, zeolite and carbon materials[44] have been developed to remove colored organic pollutants. Yet, challenging issues like relatively low removal efficiency and separation difficulty still remain for most conventional adsorbents.

1.6.1 Clay

Clay or nanoclay filled polymer nanocomposites represent a new class of materials, which have attracted much attention because of their excellent physical properties such as high dimensional stability, gas barrier performance, flame retardancy, and mechanical strength when compared to the pure polymer or conventional composites (micro and macro composites). In nanocomposites nanoclays are used because of its natural abundance and very high form factor. Two types of clays like natural or synthetic are used as nanoplate fillers. Various natural and synthetic nanoclays including Kaolinite, Smectite,(Talc, Mica, Mommorillonite), Sepiolite, Saponite, FluoroHectorite, Zeolite, Kenyaite, Magadiite, Kanemite, Ilerite, Silhydrite etc. are widely used as nanofiller in nanocomposite [45,46]. They are normally shell shaped crystalline structure with nanometric thickness.

1.6.2 Zeolite

Zeolite molecular sieves are crystalline, highly porous materials, which belong to the class of aluminosilicates. These crystals are characterized by a three-dimensional pore system, with identical pores of precisely defined diameter. This structure is formed by tetrahedras of (AlO₄) and (SiO₄). These tetrahedras are the basic building blocks for various zeolite structures, such as zeolites A and X, the most common commercial adsorbents [53]. Natural zeolites are abundant and low cost resources, which are crystalline hydrated aluminosilicates with a framework structure containing pores occupied by water, alkali and alkaline earth cations. Due to their high cation-exchange ability as well as to the molecular sieve properties, natural zeolites have been widely used as adsorbents in separation and purification processes in the past decades [54].

1.6.3 Activated Carbon

Activated carbon is the most uses adsorbent. Over the centuries the ability of charcoal to remove odor and taste was observed. According to the Sanskrit manuscript from circa 200 BC,” it is good to keep water in copper vessels, to expose it in sunlight and to filter it through charcoal.” [47, 48]. However, the credit of developing commercial activated carbon goes to Raphael von Ostrezko [49]. Activated carbon is porous material which is commercially used for the removal of liquids and gases

pollutants owing to its large surface area. It is a carbonaceous adsorbent and has known to have highly amorphous structure [50]. It has been observed that adsorption on activated carbon is not usually selective as it occurs through weak Van der Waals forces [5]. In 2009, the study of preparation of activated carbon from digested sludge of the tannery industry was done for the removal of a reactive dye [51]. The experimental data correlated well with the Langmuir, Freundlich and Temkin adsorption isotherms. In 2011, the study was done on the ability of activated carbon in the removal of two anionic dyes (Direct Blue 78 and Direct Red 31) from colored wastewater in single and binary systems [52].

1.7 Magnetic Adsorbent

The magnetic nanocomposite materials has been the source of discovery of spectacular new phenomena, with possible applications in different fields. Magnetic nanoparticles (MNPs) have gained great attention for its intrinsic magnetic properties, the broad spectrum of nanoscale materials being investigated for various environmental and biomedical applications, its magnetic property makes it successful as magnetically separable catalysts, drug delivery agents, anticancer materials, magnetic resonance imaging devices, etc. Magnetic nanoparticles and nanocomposites have aroused significant scientific and technological interest because of their potential applications in the fields of biomedicine, information technology, magnetic resonance imaging, catalysis, telecommunication, and environmental remediation [23–26]. Magnetic polymer nanocomposites generally comprise of magnetic nanoparticles embedded in polymer matrix. However, magnetic nanoparticles dispersed in composites usually have a strong tendency to form agglomerates for reduction of energy associated with high surface area-to-volume ratio of the nanosized particles. To avoid aggregation of magnetic nanoparticles, protection strategies have been developed to chemically stabilize the magnetic nanoparticle. The properties of magnetic particles remain same after stabilization. So its application in polymer nanocomposites is increasing day by day.

1.7.1 Three dimensional crosslinker

This class of crosslinkers added new dimension in the crosslinked composite materials. The shape of the 3D crosslinker may be spherical. Its surface area is comparatively higher than that of the linear or planar crosslinker. In case of 2D

crosslinker only two sides contain active sites for the interaction with substrate but in case of 3D crosslinker, reactive sites are laying all sides of 3D crosslinker. Hence it contains a wide number of reactive sites in a small surface area. Due to this its reactivity increases dramatically. Since reactive sites are scattered, 3D crosslinkers are able to link with much more polymer chains. As a result the produced nanocomposite become robust and improved chemical and mechanical properties of the nanocomposites.

1.7.2 Carboxylated Cellulose nanocrystals (CCN)

As CNC has high crystallinity, dispersive property and great mechanical strength, it exhibits multidimensional application in different fields. But in case of wastewater management, the application of CNCs is much less explored because it aggregates due to the formation of tightly hydrogen bonded networks as the surface of CNC has numerous hydroxyl groups. The aggregation of CNC can be reduced by surface modification. Generally the surface of CNCs is modified by esterification, etherification, oxidation, amidation, carbamation, nucleophilic substitution, silylation, polymer grafting, etc. by introducing negative or positive charge on the surface of CNC provides better dispersion in any solvent. By oxidation reaction surface hydroxyl group converted to carboxyl group which ultimate produce negative charge on the surface. Carboxyl group containing CNC is called CCN, which acts as efficient adsorbent for removal of dye and heavy metals. Recently, 2, 2, 6, 6-tetramethylpiperidine-1-oxyl radical (TEMPO) mediated oxidation [64-67], periodate-chlorite oxidation [55–59] and ammoniumpersulfate (APS) oxidation [60,61] have been used to produce CCN. Cross sectional representation of cellulose nanocrystal indicating the occurrence of the surface TEMPO-mediated oxidation of available hydroxyl groups Cross sectional representation of cellulose nanocrystal indicating the occurrence of the surface TEMPO-mediated oxidation of available hydroxyl groups

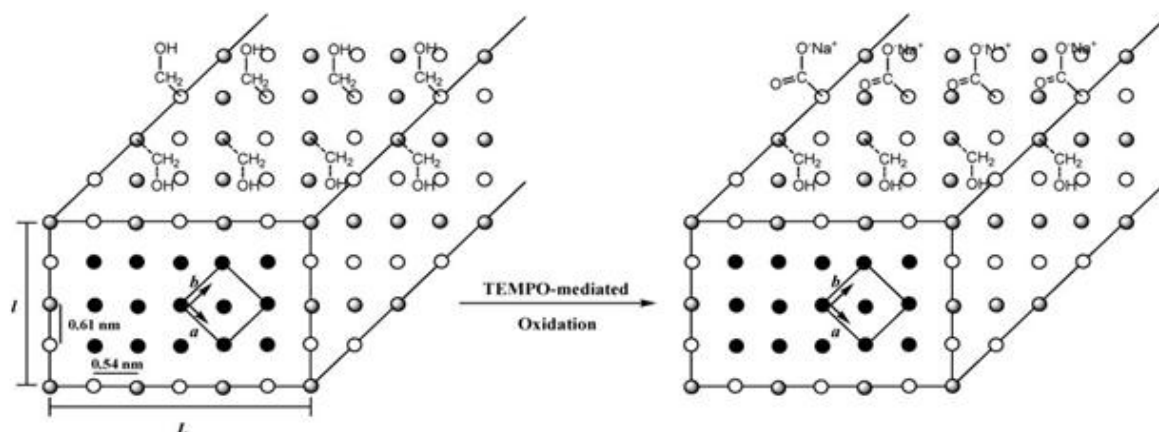


Fig.1.7.2 Cross sectional representation of cellulose nanocrystal indicating the occurrence of the surface TEMPO-mediated oxidation of available hydroxyl groups

In case of periodate-chlorite treatment of CNC, periodate selectively oxidize C₂ and C₃ hydroxyl groups to two aldehyde groups and then to carboxyl groups. During periodate treatment it breaks down the pyranose ring of the glucose unit and may decrease molecular chain lengths or rigidity of the CNCs [57, 58, 62]. Periodate is toxic as well as expensive and as it is two step process, it requires more time. On the other hand TEMPO mediated oxidation selectively oxidize C₆ hydroxyl group to carboxyl group and it is one step process; it requires comparatively lesser time and the pyranose ring remains intact. As a result, rigidity of CCNs remains same with CNCs after carboxylation of CNCs.

1.7.3 Magnetically responsive polymer composite

During the last decade, the development of magnetic polymer nanocomposite materials has been the source of discovery of spectacular new phenomena, with potential applications in the multidimensional fields. Among the broad spectrum of nanoscale materials being investigated for various environmental and biomedical applications, magnetic nanoparticles (MNPs) have gained significant attention due to their intrinsic magnetic properties, which makes them successful as magnetically recoverable catalysts, drug delivery agents, anticancer materials, magnetic resonance imaging devices, etc. Magnetic nanoparticles and nanocomposites have aroused significant scientific and technological interest because of their potential applications

in the fields of biomedicine, information technology, magnetic resonance imaging, catalysis, telecommunication, and environmental remediation [3–6]. Magnetic polymer nanocomposites generally comprise of magnetic nanoparticles embedded in polymer matrix. However, magnetic nanoparticles dispersed in composites usually have a strong tendency to form agglomerates for reduction of energy associated with high surface area-to-volume ratio of the nanosized particles. To avoid aggregation of magnetic nanoparticles, protection strategies have been developed to chemically stabilize the magnetic nanoparticle. The properties of magnetic particles remain same after stabilization. So its application in polymer nanocomposites is increasing day by day.

1.8 Research Goal

Different types of physical, chemical and biological de-colorization methods such as coagulation/ flocculation treatment, biodegradation processes, oxidation methods, membrane filtration and adsorption have been reported to be investigated for the removal of dyes from industrial effluents [9-12]. Among the studied methods, removal of dyes from adsorption is found to be the most competitive one because it does not need a high operating temperature and several coloring materials can be removed simultaneously [1]. The versatility of adsorption is due to its high efficiency, economic feasibility and simplicity of design [4]. As there are various parameters to effect adsorption process such as, charge density and structural stability of the adsorbent so, in the thrust of a comprehensive study, we have selected basic dye Methylene blue for this present study.

CHAPTER 7 Herein, we use a novel composite of magnetite crosslinked poly(acrylic acid) (Fe_3O_4 -PAA) and carboxylated cellulose nanocrystal (CCN) as an adsorbent, which is easily magnetically separable after the treatment, for the removal of cationic dye such as methylene blue.

In this research, the main reasons of using nanocomposite containing 3D crosslinker and cellulosic material. Because When nanocomposite used as adsorbent, there is a challenging issue to separate them. The separation of nonmagnetic nanocomposite after using as adsorbent is very complex, lengthy and tedious. Magnetic

nanocomposite is an excellent nanomaterials for wastewater management due to its easy separation process and its demand increasing day by day. From the literature review it was seen that magnetic nanocomposites contain magnetic nanoparticles embedded on the polymer matrix and they were loosely bound to the polymer chain with van der Waal force. When the magnetic field is applied then only the magnetic particles attracted by the magnet and separate leaving the polymer chain as the polymer chains are not directly linked with magnetic particles. So the nanocomposites are not possible to recycle or reuse. Hence this type of nanocomposite can use only one time. As a result its usage is expensive. Nanocomposites can be recycled and reused if the magnetic particles are directly linked with the polymer chains. Herein, we plan to modify magnetic particles by acrylic group and this acrylic group directly linked with polymer chain by strong covalent bond. This acrylic modified magnetic particles act as 3D crosslinker which has more reactive sites than conventional linear or planar crosslinker and resulting make the composite much more sticky and adhesive. So another approach is to decrease this adhesive property and increase dispersive property. For this purpose, carboxylated cellulose nanocrystals, which are highly dispersive in most of the solvent, are incorporated in the composite. Finally, more reactive sites containing 3D crosslinker, highly dispersive carboxylated cellulose nanocrystals and acrylic acid monomer are used to synthesize a new magnetic nanocomposite via in situ polymerization using potassium per sulfate as initiator.

The synthesized nanocomposite will be tested for the adsorption of methylene blue and the kinetics data will be fitted to pseudo-first-order and pseudo-second-order models to figure out the adsorption mechanism. The adsorption capacity of MB on nanocomposite will be investigated in batch process [8]. The effects of pH on the adsorption of MB will be investigated by monitoring the kinetics at variable pH. Adsorption processes of MB on PAA/ Fe_3O_4 / CCN (PAAMCCN) will be tested using different isotherm models by varying the concentration of the adsorbent.

References.

1. G.Crini., “Non-conventional low-cost adsorbents for dye removal a review”, *Bioresour, Technol.* Vol. 97, pp. 1061-1085 (2006).
2. B. Dash, “Competitive adsorption of dyes (congo red, methylene blue, malachite green) on activated carbon”, *B.Tech thesis*, 2010.
3. A. Mittal., A. Malviya., D. Kaur., J. Mittal., L. Kurup, “Studies on the adsorption kinetics and isotherms for the removal and recovery of Methyl Orange from wastewaters using waste materials”, *J. Hazard, Mater.* Vol. 148, pp. 229-240 (2007)
4. S. Chen., J. Zhang., C. Zhang., Q. Yue., Y. Li., C. Li., “Equilibrium and kinetics studies of methyl orange and methyl violet adsorption on activated carbon derived from phragmitesaustralis”, *Desalination* Vol. 252, pp. 149-156 (2010).
5. V. K. Gupta., Suhas., “Application of low-cost adsorbents for dye removal-a review”, *J. Environmental Management* Vol. 90, pp. 2313-2342 (2009).
6. C. I. Pearce., J. R. Lloyd., J. T. Guthrie., “The removal of colour from textile wastewater using whole bacteria cells: a review”, *Dyes pigments.*, Vol. 58, pp. 179-196 (2003).
7. T. Robinson., G. McMullan., R. Marchant., P. Nigam., ‘Remediation of dyes in textile effluent: a critical review on current treatment technologies with a proposed alternatives’, *Bioresour, Technol.* Vol. 77, pp. 247-255 (2001).
8. J. Zhang., M. S. Azam., C. Shi., J. Huang., B. Yan., Q. Liu., and H. Zeng., “Poly(acrylic acid) functionalized magnetic graphene oxide nanocomposite for removal of methylene blue,” *RSC Advances*, Vol. 5, pp. 32272-32282 (2015).
9. Y. Anjanyeulu., N. Sreedhara., D. Chary., S.R. Samuel., “De-colourization of industrial effluents-available methods and emerging technologies- a review”, *Rev. Environ. Sci. Biotechnol.* Vol. 4. pp. 245-273 (2005).
10. H. Singhrai., M.S. Bhattacharyya., J. Singh., T.K. Bansal., P. Vats., U.C. Banerjee., “Removal of dyes from the effluent of textile and dyestuff manufacturing industry: a review of emerging techniques with reference to biological treatment”, *Crit. Rev. Environ. Sci. Technol.* Vol. 35, pp. 219-235 (2005).
11. G. Crini., P. M. Badot., N. M. Crini., G. Torri., “Wastewater treatment processes: a recent review of the available methods”, *in: Press universitaires de Franche-Comte (PUFC)*, pp. 16-62 (2007).

12. F. Gimbert., N. M. Crini., F. Renault., P. M. Badot., G. Crini., “Adsorption isotherm models for dye removal by cationized starch-based material in a single component system: error analysis”, *J. Hazard. Mater.*, Vol. 157, pp. 34-46 (2008).
13. R. M. Christie, “Environmental aspects of textile dyeing, Woodhead”, *Boca Raton, Cambridge*, (2007).
14. K. Hunger., “Industrial dyes: chemistry, properties, applications”, *Wiley-VCH, Weinheim, Cambridge*, (2003).
15. K. Venkataraman, “The chemistry of synthetic dyes”, *Academic press Inc., New York*, (1965).
16. W. L. McCabe., J. C. Smith., P. Harriot., “Unit operations of chemical engineering”, *McGraw-Hill*, Singapore (2005).
17. I. A. Aguayo-Villarreal., V. Hernández-Montoy., A. Bonilla-Petriciolet., R. Tovar-Gómez., E.M. Ramírez-López., M.A. Montes-Morán., “Role of acid blue 25 dye as active site for the adsorption of Cd²⁺ and Zn²⁺ using activated carbons”.
18. A. Mansoor., S. Samira., “Removal of acid dyes from aqueous media by adsorption onto amino-functionalized nanoporous silica SBA-3”
19. N. M. Mahmoodi., R. Salehi., M. Arami., H. Bahrami., “Dye removal from colored textile wastewater using chitosan in binary systems”, *Desalination* Vol. 267, pp. 64-72 (2011).
20. S. A. Saad., Md. K. Isa, R. Bahari., “Chemically modified sugarcane bagasse as a potentially low- cost biosorbent for dye removal”, *Desalination* Vol.264 , pp. 123-128 (2010).
21. D. Sun., X. Zhang., Y. Wu., X. Liu., “Adsorption of anionic dyes from aqueous solution on fly ash”. *J. Hazard. Mater.* Vol. 181, pp. 335-342 (2010) .
22. Q. Liu., L. Wang., A. Xiao., J. Gao., W. Ding., H. Yu., J. Huo., M. Ericson., “Templated preparation of porous magnetic microspheres and their application in removal of cationic dyes from wastewater”, *J. Hazard. Mater.* Vol.181, pp.586-593 (2010).
23. M. Jafarbeglou., M. Abdouss., A. M. Shoushtari., M. Jafarbeglou., “Clay nanocomposites as engineered drug delivery systems”, *RSC Adv.*, vol. 6, pp. 50002-50016 (2016).

24. R. I. Iliescu., E. Andronescu., C. D. Ghitulica., G. Voicu.,, A. Fikai., M. Hoteteu., “Montmorillonite–alginate nanocomposite as a drug delivery system – incorporation and in vitro release of irinotecan”, *Int. J. Pharma.*, Vol. 463, pp. 184–192 (2014).
25. W. E. Jones., J. Chiguma., E. Johnson., A. Pachamuthu., D. Santos., “Electrically and Thermally Conducting Nanocomposites for Electronic Applications”, *Materials*, Vol. 3, pp. 1478-1496 (2010).
26. https://en.wikipedia.org/wiki/Nanocomposite#Ceramic-matrix_nanocomposites. [Last access on 15 Nov. 2017].
27. J. Jancar., J. F. Douglas., F. W. Starr., S. K. Kumar, P. Cassagnau., A. J. Lesser., S. S. Sternstein., M. J. Buehler., “Current issues in research on structure-property relationships in polymer nanocomposites,” *Polymer*, Vol. 51, pp. 3321–3343 (2010).
28. N. Chandrasekara., R. Pashley., “Study of a new process for the efficient regeneration of ion exchange resins,” *Desalination*, Vol. 357, pp. 131–139, (2015).
29. X. Xu., B. Bai., C. Ding., H. Wang., Y. Suo., “Synthesis and properties of an ecofriendly superabsorbent composite by grafting the poly (acrylic acid) onto the surface of dopamine-coated sea buckthorn branches,” *Industrial & Engineering Chemistry Research*, vol. 54, pp. 3268–3278 (2015).
30. H. Y. Zhu., Y. Q. Fu., R. Jiang., J. H. Jiang., L. Xiao., G. M. Zeng., S. L. Zhao., Y. Wang., “Adsorption removal of congo red onto magnetic cellulose/Fe₃O₄/activated carbon composite: Equilibrium, kinetic and thermodynamic studies,” *Chemical Engineering Journal*, vol. 173, pp. 494–502 (2011).
31. J. Yan ., Y. Huang., Y. E. Miao., W. W. Tjiu., T. Liu., “Polydopamine-coated electrospun poly (vinyl alcohol)/poly(acrylic acid) membranes as efficient dye adsorbent with good recyclability,” *Journal of Hazardous Materials*, vol. 283, pp. 730–739 (2015).
32. J. Zhang., M. S. Azam., C. Shi., J. Huang., B. Yan., Q. Liu., H. and Zeng. , “Poly(acrylic acid) functionalized magnetic graphene oxide nanocomposite for removal of methylene blue,” *RSC Advances*, vol. 5, pp. 32272-32282 (2015).
33. H. Yana., L. Yanga., Z. Yanga., H. Yanga., A. Li. , Chenga R., “Preparation of chitosan/poly(acrylic acid) magnetic composite microspheres and applications in the removal of copper(II) ions from aqueous solutions,” *Journal of Hazardous Materials*, vol. 229–230 pp. 371–380 (2012).

34. Y. Anjaneyulu., N.S. Chary., and D.S.S. Raj., “Decolourization of industrial effluent savailable methods and emerging technologies-a review,” *Reviews in Environmental Science and Biotechnology.*, Vol. 4, pp. 245-273 (2005).
35. V. Golob., A. Vinder., and M. Simonic., “Efficiency of coagulation/flocculation method for treatment of dye bath effluents,” *Dyes and Pigments.*, Vol. 67, pp. 93-97 (2005).
36. F.I. Hai., K. Yamamoto., and K. Fukushi., “Hybrid treatment systems for dye wastewater,” *Critical Reviews in Environmental Science and Technology.*, Vol. 37, pp. 315-377 (2007).
37. H. Dong., G. Zeng., L. Tang., C. Fan., C. Zhang., X. He., Y. He., “An overview on limitations of TiO₂-based particles for photocatalytic degradation of organic pollutants and the corresponding countermeasures”, *Water Research* (2015)
38. M. Marcucci., G. Nosenzo., G. Capannelli., I. Ciabatti., D. Corrieri., and G. Ciardelli., “Treatment and reuse of textile effluents based on new ultrafiltration and other membrane technologies,” *Desalination.*, Vol. 138, pp. 75-82 (2001).
39. C. Fersi., and M. Dhahbi., “Treatment of textile plant effluent by ultrafiltration and/ or nanofiltration for water reuse,” *Desalination.*, Vol. 222, pp. 263-271 (2008).
40. S. Ledakowicz., M. Solecka., and R. Zylla., “Biodegradation, decolourisation and detoxification of textile wastewater enhanced by advanced oxidation processes,” *Journal of Biotechnology.*, Vol. 89, pp. 175-184 (2001).
41. A.L. Ahmad., W. A. Harris., and B. S. Syafie., “Removal of dye from wastewater of textile industry using membrane technology,” *Universiti Teknologi Malaysia Jurnal Teknologi.*, Vol. 36 (F), pp. 31-44 (2002).
42. T. Robinson., G. McMullan., R. Marchant, and P. Nigham., “Remediation of dyes in textile effluent: a critical review on current treatment technologies with

proposed alternatives,” *Bioresource Technology*, Vol. 77, pp. 247-255 (2001).

43. A. Akbari., S. Desclaux., J.C. Rouch., P. Aptel., and J.C. Remigy., “New UVphotografted nanofiltration membranes for the treatment of colored textile dye effluents,” *Journal of Membrane Science*, Vol. 286, pp. 342-350 (2006).

44. B. Hameed., A. M. Din., and A. Ahmad., “ Adsorption of methylene blue onto bamboo-based activated carbon: Kinetics and equilibrium studies,” *Journal of Hazardous Materials*, vol. 141, pp. 819–825 (2007).

45. T. Liu., K. P. Lim., W.C. Tjiu., K. P. Pramoda., Z. K. Chen., “Preparation and characterization of nylon 11/organoclay nanocomposites”. *Polymer*, vol. 44, pp. 3529–3535, 2003.

46. A. Lateef., R. Nazir., N. Jamil., S. Alam., R. Shah., M. N. Khan., M. Saleem., “Synthesis and characterization of zeolite based nano-composite: An environment friendly slow release fertilizer”, *Micropor. Mesopor. Mater.*, vol. 232, pp. 174–183 (2016).

47. H. M. Freeman., “Standard handbook of hazardous waste treatment and disposal”, *second ed. McGraw-Hill*, New York (1989).

48. C. Tein., “Adsorption calculations and modeling”, *Butterworth-Heinemann*, Boston (1994).

49. M. Smisek., S.Cerny., “Active carbon manufacture properties and applications, Elsevier publishing company”, Amsterdam (1970).

50. R.C. Bansal., M. Goyal., “Activated carbon adsorption”, London, Taylor and Francis group, LLC (2005).

51. S. Govidasami., B.R.P. Kumar., C. Balamurli Krishna., R. Mayildurai., “Equilibrium and isotherm studies of sludge based activation carbon”, *Ecol. Environ. Conserv.* Vol.15, pp.817-824 (2009).
52. N. M. Mahmoodi., R.Salehi., M.Arami., “Binary system dye removal from colored textile waste water using activated carbon: kinetic and isotherm studies”, *Desalination* Vol.272, pp. 187-195 (2011).
53. R. Grace & Co. Enriching Lives, “Everywhere. – Zeolite Structure” Archived February 15, 2009, at the Wayback Machine.. Grace.com. Retrieved on 2010.
54. W. Shaobin., P. Yuelian., “Natural zeolites as effective adsorbents in water and wastewater treatment” *Chemical Engineering Journal*, vol. 156, pp. 11-24 (2010) .
55. N.Drogat., R. Granet., V. Sol., A. Memmi., N.Saad., C. K.Koerkamp., P.Bressollier., P.Krausz., “Antimicrobial silver nanoparticles generated on cellulose nanocrystals”. *J. Nanopart. Res.*, vol. 13(4), pp. 1557-1562 (2011).
56. M. Visanko., H. Liimatainen., J. A. Sirviö., J. P. Heiskanen., J. Niinimäki., O. Hormi., “Amphiphilic cellulose nanocrystals from acid-free oxidative treatment: physicochemical characteristics and use as an oil-water stabilizer”. *Biomacromol.*, vol. 15 (7), pp. 2769-2775, (2014).
57. B. Sun., Q. Hou., Z. Liu., Y. Ni., “Sodium periodate oxidation of cellulose nanocrystal and its application as a paper wet strength additive”. *Cellulose*, vol. 22 (2), pp. 1135-1146 (2015).
58. H. Liimatainen., M. Visanko., J. Sirviö, O. Hormi., J. Niinimäki., “Sulfonated cellulose nanofibrils obtained from wood pulp through regioselective oxidative bisulfate pre-treatment”. *Cellulose*, vol. 20 (2), pp. 741-749 (2013).
59. H. Liimatainen., M. Visanko., J. Sirviö., O. Hormi.,J. Niinimäki.,“Enhancement of the nanofibrillation of wood cellulose through sequential periodate-chlorite oxidation”, *Biomacromol.*, vol. 13 (5), pp. 1592-1597(2012).
60. M. Cheng., Z. Qin., Y. Liu., Y. Qin., T. Li., L. Chen., M. Zhu.,“Efficient extraction of carboxylated spherical cellulose nanocrystals with narrow distribution

through hydrolysis of lyocell fibers by using ammonium persulfate as an oxidant”, *J. Mater. Chem. A*, vol. 2 (1), pp. 251-258 (2014).

61. A. C. Leung., S. Hrapovic., E. Lam., Y. Liu., K. B. Male., K. A. Mahmoud., J. H Luong., “Characteristics and properties of carboxylated cellulose nanocrystals prepared from a novel one-step procedure”, *Small*, vol. 7(3), pp. 302-305 (2011).

62. T. Saito., A. Isogai., “TEMPO-mediated oxidation of native cellulose. The effect of oxidation conditions on chemical and crystal structures of the water-insoluble fractions”, *Macromol.*, vol. 5 (5), pp. 1983-1989 (2004).

63. R. Batmaz., N. Mohammed., M. Zaman., G. Minhas., R. M. Berry., K. C. Tam., “Cellulose nanocrystals as promising adsorbents for the removal of cationic dyes”, *Cellulose*, vol. 21 (3), pp. 1655-1665 (2014).

64. Y. Wang., L. Chen., “Cellulose nanowhiskers and fiber alignment greatly improve mechanical properties of electrospun prolamin protein fibers”. *ACS Appl. Mater. Inter.*, vol. 6 (3), pp. 1709-1718 (2014).

65. N. Lin., C. Bruzzese., A. Dufresne., “TEMPO-oxidized nanocellulose participating as crosslinking aid for alginate-based sponges”. *ACS Appl. Mater. Inter.*, vol. 4 (9), 4948-4959 (2012).

66. J. Peyre., T. Pääkkönen., M. Reza., E. Kontturi., “Simultaneous preparation of cellulose nanocrystals and micron-sized porous colloidal particles of cellulose by TEMPO-mediated oxidation”. *Green Chem.*, vol. 17 (2), pp. 808-811 (2015).

67. F. Rafieian., M. Shahedi., J. Keramat., J. Simonsen., “Mechanical, thermal and barrier properties of nano-biocomposite based on gluten and carboxylated cellulose nanocrystals”. *Int. Crop. Prod.*, vol. 53, pp. 282-288 (2014).

68. M. Iram., C. Guo., Y. Guan., A. Ishfaq., and H. Liu., “Adsorption and magnetic removal of neutral red dye from aqueous solution using Fe₃O₄ hollow nanospheres,” *J. Hazard. Mater*, Vol. 181, pp. 1039-1050 (2010).

CHAPTER 2

Experimental

2.1 Chemical and reagents

The chemicals and reagents used in this research were analytical grade and used without further purification. Distilled water was used as solvent to prepare most of the

solutions of this work. The chemicals and reagents which were used in this research are given below:

- i. Ethanol (Merck, Germany)
- ii. Toluene (Merck, Germany)
- iii. Sodium chlorite (BDH)
- iv. Sodium hydroxide (Merck, Germany)
- v. Sodium hypochlorite (Merck, Germany)
- vi. Sodium bromide (Loba, India)
- vii. Potassium hydroxide (Merck, India)
- viii. Potassium per sulfate (BDH)
- ix. Sulfuric acid (Merck, Germany)
- x. Hydrochloric acid (analytical grade)
- xi. 2,2,6,6-Tetramethylpiperidine-1-oxyl (TEMPO)
- xii. Acetone (analytical grade)
- xiii. Ferrous chloride $4\text{H}_2\text{O}$ (Sigma Aldrich)
- xiv. Ferric chloride $6\text{H}_2\text{O}$ (Sigma Aldrich)
- xv. Ammonia solution (25%)
- xvi. Tetraethylorthosilicate (TEOS) (Sigma Aldrich)
- xvii. 3-aminopropyltriethoxysilane (APTES) (Sigma Aldrich)
- xviii. N,N'-diethylformamide (DMF) (Merck, Germany)
- xix. Methacrylic anhydride (Sigma Aldrich)

- xx. Acrylic acid (BDH)
- xxi. Methylene Blue (Merck, India)

2.2 Instruments

Analysis of the samples was performed using the following instruments:

- i. Fourier Transform Infrared Spectrophotometer (SHIMADZU FTIR-8400)
- ii. Field Emission Scanning Electron Microscopy (JSM-7600F, Tokyo, Japan)
- iii. X-ray Diffractometer (Philips, Expert Pro, Holland)
- iv. X-ray photoelectron Spectroscopy
- v. Thermogravimetric analyser (TGA 50-H)
- vi. Centrifuge machine (Hettich, Universal 16A)
- vii. pH meter (Hanna, HI 8424, Romania)
- viii. Digital Balance (AB 265/S/SACT METTLER, Toletto, Switzerland)
- ix. Freeze dryer (Heto FD3)
- x. Oven (Lab Tech, LDO-030E)
- xi. Magnetic Stirrer (Snijders)
- xii. UV-Visible Spectrophotometer (Shimadzu-1800)

2.3 Synthesis of magnetic nanocomposite

2.3.1 Synthesis of acrylated magnetic iron oxide nanoparticles

2.3.1.1 Synthesis magnetic iron oxide nanoparticles (Fe₃O₄)

The magnetic iron oxide nanoparticles (Fe_3O_4) were prepared by the most common, easy and widely used, chemical co-precipitation method [5]. Firstly, an iron salt solution was obtained by mixing 0.005 mol 2.703g FeCl_3 and 0.0025 mol 0.6336g FeCl_2 such that the ratio of Fe^{3+} to Fe^{2+} becomes 2 in 50 mL distilled water which is deoxygenated by passing N_2 gas about 10 min. 20 mL of 1.5M NaOH was rapidly poured into the iron salt solution under vigorous magnetic stirring at room temperature (RT). Orange color of the iron salt solution was instantly changed and black precipitate was found. After continuously stirring for 20 min, the precipitate was separated magnetically and then washed with distilled water for several times by centrifugation.

2.3.1.2 Synthesis Silica Coated magnetic iron oxide nanoparticles

The magnetic iron oxide nanoparticles (Fe_3O_4) were coated with silica by hydrolysis of tetraethylorthosilicate (TEOS) in basic solution via Stöber's method [6]. In this case, 300 mg magnetite nanoparticles were dispersed into a mixture of 240 mL ethanol and 60 mL distilled water and sonicated for 15 min. The pH value was adjusted to 9 with 25% ammonia solution and 4 mL TEOS was added under vigorous stirring. The resulting dispersion was mechanically stirred for 10 hour at room temperature. For complete hydrolysis, the sample was heated at 50 °C for 12 hour. After cooling the sample, solvent was removed by centrifugation, and then the sample was washed with anhydrous ethanol and later washed with dimethyl formamide (DMF).

2.3.1.3 Synthesis Aminated magnetic iron oxide nanoparticles

DMF washed silica-coated Fe_3O_4 were ultrasonically redispersed into a solution containing 120 mL DMF and 80 mL toluene, then taken into a double-necked RB flask. 10 mL (3-aminopropyl) triethoxysilane (APTES) was added dropwise under magnetic stirring. After hydrolysis for 24 h at room temperature, the particles were separated by centrifugation and washed with toluene several times.

2.3.1.4 Synthesis Acrylated magnetic iron oxide nanoparticles (3D)

The sample was then taken into 250 mL RB flask containing 150 mL toluene and heated at 120 °C until the sample volume became 90 mL. After reaching that volume heating stopped and kept for cool down at room temperature. Always covered the flask tightly because water absorbed by the sample. After that 6.7 mL methacrylic

anhydride was added to the sample and magnetically stirred about 4 hours. Finally, the sample was washed with toluene several times and kept in toluene and got acrylic modified magnetic iron oxide nanoparticles. It is very essential to keep the sample into water for future reaction. For this solvent exchange needed from toluene to water. Toluene and water are practically insoluble in each other. Toluene and acetone are miscible in all proportions, as are also acetone and water. For this reason acetone was added to sample in toluene and after that solvent was removed. This was repeated several times and as a result toluene was almost completely removed. After that, water was added to the sample in acetone. This was repeated several times and the sample was heated at 58 °C. As a result, acetone was completely removed and the sample retained in water.

2.3.2 Synthesis of carboxylated cellulose nanocrystals (CCN)

The primary hydroxyl groups on the surface of CNC were oxidized to carboxyl groups using TEMPO-reagent in the presence of sodium bromide (NaBr) and sodium hypochlorite (NaClO). The reaction conditions were adjusted by the previous studies [2, 3, 4]. 1g CNC was dispersed in 100 mL distilled water. After mixing, sonication was performed for 10 min in ice bath to get a homogeneous dispersion of CNC. 16 mg TEMPO and 100 mg NaBr was weighed and dissolved separately. After that mixed with CNC suspension and stirred 10 min at room temperature.

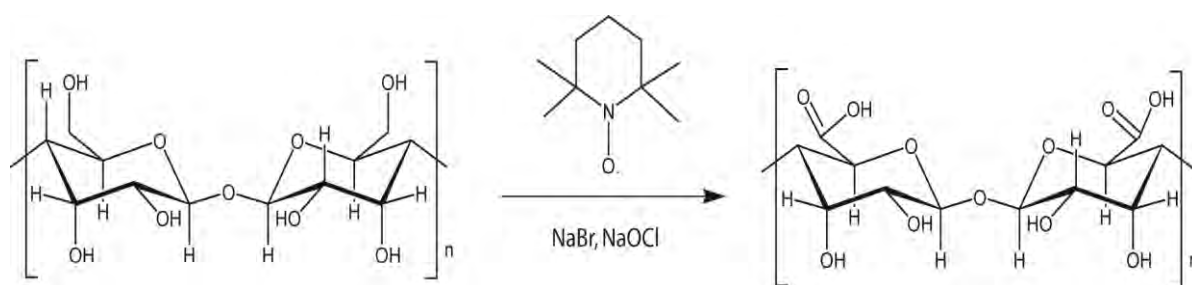


Figure 2.1 Schematic representation of carboxylated cellulose nanocrystals

This was further sonicated for 15min. The oxidation was initiated with the addition of 3.5 mL of 4-14% NaClO solution to the CNC suspension by dropwise. The pH of the solution was maintained constant at 10 by adding 0.1M NaOH solution until no more variation was observed, indicating that the reaction was finished. Then the solution

was continuously stirred for 12 h. Finally, 5 mL of ethanol was added to stop the oxidation. Then the solution was washed with distilled water several times and finally obtained concentrated suspension which was sonicated for 2 min and stored at 4 °C.

2.3.3 Synthesis of nanocomposite

PAA/Fe₃O₄/CCN (PAAMCN) nanocomposite was synthesized via *in situ* polymerization process. 36 mg of CCN and 14 mg of acrylated Fe₃O₄ was taken into a beaker individually containing 10 mL distilled water and sonicated for 5 min in an ice bath and the temperature kept below 20 °C. After that CCN and coated magnetic iron oxide was mixed and further sonicated for 15 min. 25 mg of potassium persulfate (KPS) was taken into 5 mL distilled water and dissolved properly. 1 mL acrylic acid was added dropwise at 12 °C under sonication in ice bath. Finally free radical polymerization was allowed to continue by adding KPS solution dropwise. This mixture was heated at 58 °C and continuously stirring at 1200 rpm for 4 hours. After completion of the reaction, resulting nanocomposite was washed with distilled water several times and dried with freeze dryer.

2.4 Sample characterization

2.4.1 Fourier transform infrared analysis (FTIR)

The infrared spectra of the cellulose nanocrystal, carboxylated cellulose nanocrystal, magnetic iron oxide nanoparticle Fe₃O₄, Silica coated Fe₃O₄, aminated Fe₃O₄, acrylated Fe₃O₄ and nanocomposite samples were recorded on an FTIR spectrometer in the region of 4000 – 400 cm⁻¹. A small portion of cellulose nanocrystal and carboxylated CNC (CCN) was taken into vial and oven dried at 80 °C. After that it was cut as much as possible small sized pieces and then grinded as much as possible. On the other hand magnetic iron oxide nanoparticles, silica coated magnetic iron oxide nanoparticles, aminated Fe₃O₄, acrylated Fe₃O₄ were dried and grinded into a mortar with a pestle. The powder mixture was then compressed in a metal holder under a pressure of 8–10 tons to make a pellet. The pellet was then placed in the path of IR beam for measurements.

2.4.2 Field emission scanning electron microscopy (FE-SEM)

The surface morphology of the synthesized CNC, CCN, magnetic iron oxide nanoparticles (Fe₃O₄), silica coated Fe₃O₄ aminated Fe₃O₄, acrylated Fe₃O₄,

PAA/Fe₃O₄/CCN (PAAMCCN) nanocomposite was adopted using Field Emission Scanning Electron Microscopy (FE-SEM). Glass substrate was used for the sample preparation of Fe₃O₄, acrylated Fe₃O₄ and nanocomposite. The concentration was 0.0001%. One drop of dilute sample was taken on the surface of glass and air dried. But in case of CNC and CCN, silicon substrate was used. 0.05% CNC and CCN was taken on the surface of silicon substrate and the freeze dried about 24 hour. The sample loaded substrate was then mounted to a chamber that evacuated to $\sim 10^{-3}$ to 10^{-4} tor and then a very thin platinum layer (few nanometers thick) were sputtered on the sample to ensure the conductivity of the sample surface. The sample was then placed in the main FE-SEM chamber to view its surface. The microscope was operated at an accelerating voltage of 5.0 kV.

2.4.3 Energy dispersive x-ray (EDX) spectra

Elemental analyses of the synthesized CNC, CCN, Fe₃O₄, silica coated Fe₃O₄, acrylated Fe₃O₄, nanocomposite were performed by EDX spectra. The dried powders of CNC, CCN & magnetic iron oxide nanoparticles based nanocomposite were placed on a 1 cm × 1 cm conducting steel plate. The steel plate was then placed on a conducting carbon glued strip. The sample was then placed in the main FE-SEM chamber integrated with the EDX instrument.

2.4.4 X-ray photoelectron spectroscopy (XPS)

XPS measurements were performed on samples that had been prepared within 4 days using the AXIS ULTRA spectrometer (Kratos Analytical). The base pressure in the analytical chamber was $<3 \times 10^{-8}$ Pa. The monochromatic AlK α source ($h\nu=1486.6\text{eV}$) was used at a power of 210 W. The photoelectron exit angle was 90°, and the incident angle was 35.3° from the plane of the surface. The analysis spot was 400 x 700 μm . Survey scans were collected for binding energies from 1100 to 0eV with analyzer pass energy of 160eV and a step of 0.35eV. The high-resolution spectra were run with a pass-energy of 20eV and a step of 0.1eV. Relative sensitivity factors (RSFs) for different elements were as follows: 1 for C (1s), 1.8 for N (1s), 2.93 for O (1s), 0.26 for Si (2s), 0.27 for Si (2p). Only one set of XPS scans was performed on a given sample; therefore, XPS analysis before and after surface reactions were performed on different samples.

2.4.5 Thermogravimetric analysis (TGA)

The thermal stability of CCN, acrylated Fe₃O₄, nanocomposite and 3D crosslinked poly(acrylic acid) were studied by a thermo-gravimetric analyzer (TGA) in a nitrogen atmosphere. Approximately 3-10mg freeze dried samples taken into an aluminum cell and heated from 30 to 800 °C at a heating rate of 10 °C/min under a nitrogen flow of 10 mL/ min. Before the data acquisition segment, the sample was equilibrated at 25 °C for 5 min to obtain an isothermal condition.

2.4.6 Magnetic Property Analysis

The magnetic properties of Fe₃O₄, Acrylated Fe₃O₄ and PAA/Fe₃O₄/CCN (PAAMCCN) were measured EV-9 Microsense (Germany) with an applied field between -10000 and 10000 Oe at room temperature.

2.4.7 Adsorption Experiments:

A 8 mg portion of PAA/Fe₃O₄/CCN (PAAMCCN) nanocomposite was dispersed in 1 mL of DI water (pH = 7.2). Then 50mL of methylene blue (MB) aqueous solution (pH = 7.2, 20 mg L⁻¹) added to it under stirring. The blue color of MB gradually vanished by adsorption. The adsorption process was monitored by measuring the changes in the absorbance at 665 nm at different time (i.e. 0 min, 10 min, 20 min, 30 min, 60min, 180 min, 360min, 720min, 840min) with a UV-Vis spectrophotometer. The same experiment was repeated at pH = 3.0 and pH = 9.0.

2.4.8 Zeta Potential

The effects of pH on zeta potential of Acrylated Magnetic iron oxide(3D) and PAA/Fe₃O₄/CCN (PAAMCCN) and the adsorption capacity, q , of MB on 3D and PAA/Fe₃O₄/CCN (PAAMCCN) were also investigated. with increasing pH=3 to 11.

References:

1. A. Kumar., Y. S. Negi., V. Choudhary., N. K. Bhardwaj., “Characterization of cellulose nanocrystals produced by acid hydrolysis from sugarcane bagasse as agro-waste”, *J. Mater. Physic. Chem.*, vol. 2 (1), pp. 1-8 (2014).
2. T. Saito., A. Isogai., “Cellulose nanofibers prepared by TEMPO-mediated oxidation of native cellulose”, *Biomacromol.*, vol. 8, pp. 2485-2491 (2007).
3. Y. Habibi., H. Chanzy., M.R. Vignon., “Optimization of cellouronic acid synthesis by TEMPO-mediated oxidation of cellulose III from sugar beet pulpCellulose”, vol. 13, pp. 679 (2006).
4. T. Saito., A. Isogai., “TEMPO-mediated oxidation of native cellulose. The effect of oxidation conditions on chemical and crystal structures of the water-insoluble fractions”, *Biomacromol.*, vol. 5, pp. 1983-1989 (2004).
5. Y. P. He., S.Q. Wang., C.R. Li., Y.M. Miao., Z. Y. Wu., B.S. Zou., “Synthesis and characterization of functionalized silica-coated Fe₃O₄ superparamagnetic nanocrystals for biological applications” *J. Physics D: Appl. Physic.*, vol. 38, pp. 1342–1350 (2005).
6. I. Nedkov.,, T. Merodiiska., L Slavov., R. E Vandenberghe., Y Kusano., J Takada., “Surface oxidation, size and shape of nano-sized magnetite obtained by co-precipitation” *J. Magn. Magn. Mater.*, vol. 300 (2), pp. 358–367, 2006.

CHAPTER 3

Results and Discussion

3.1 Synthesis of acrylated Fe₃O₄ (3D) crosslinker

For linking one polymer chain to another polymer chain crosslinker plays a vital role. Some crosslinkers used in commercially and some used in laboratory purpose. Among different crosslinkers 3D crosslinker has comparatively larger surface area and reactive sites than conventional liner or planar crosslinker. In this research a high performance 3D crosslinker was developed. This type of 3D crosslinker contained both magnetic and acrylic group which was able to link with polymer chain. For magnetic behavior of magnetic iron oxide nanoparticles (Fe₃O₄) were synthesized via chemical co-precipitation method. This reaction was carried out using deoxygenated water by passing N₂ gas so that produced magnetic iron oxide nanoparticles could not come in contact with air. If these nanoparticles come in contact with air, it oxidized to Fe₂O₃. As a result, the amount of Fe₃O₄ decrease and impurity incorporate which affect the further treatment. For this reason coating of nanoparticles is very essential and this essential work was done by coating with silica using tetraethylorthosilicate (TEOS) in basic medium (25% NH₃ solution). In aqueous medium polymer of silica was formed very rapidly. Anhydrous ethanol was used for controlling the reaction and for this case two step reactions was carried out. First step, after addition of TEOS stirred 10 hour without heat. Next step was carried out applying heat for 12 hours so that Si-O-Si bond break down and form Si-OH on the surface of Fe₃O₄ and completely coated.

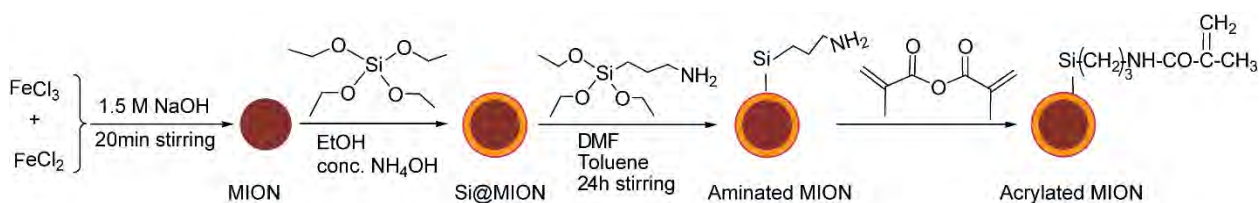


Figure. 3.1 Schematic representation of 3D crosslinker synthesis

3.2 Synthesis of carboxylated cellulose nanocrystals (CCN)

Cellulose nanocrystals (CNC) were synthesized from sawdust. Sawdust is cheap, easily available and a new source of CNC. This environmental waste material used as cheap fuel source. So for environmental safety and also for industrial purposes, CNCs extraction from sawdust creates a new dimension. CNC extracted from sawdust by acid hydrolysis process [1]. Before acid hydrolysis sawdust was pretreatment with different chemicals. The mixture of toluene and ethanol was used for the complete removal of waxy materials. Acidified sodium chlorite was used several times for the taking away of lignin, pectin and hemicelluloses. pH maintained almost neutral by centrifugation for the acid hydrolysis. Chemically purified cellulose contains both amorphous and crystalline region. Acid hydrolysis was carried out to get crystalline region. During acid hydrolysis, the hydronium ions cleaved the glycosidic linkages and thereby releasing the individual crystallites. This crystallite is known as CNC which contain negatively charged surface due to the presence of sulfate group. CNC is highly dispersive in most of the solvent. A wide range of hydroxyl groups on the surface of CNC are responsible for the tightly hydrogen bonded networks. To loosen the hydrogen bond, increase the electrostatic repulsion and adsorption ability, primary hydroxyl group of CNC was converted to carboxyl group and this carboxyl group containing CNC known as carboxylated cellulose nanocrystal (CCN).

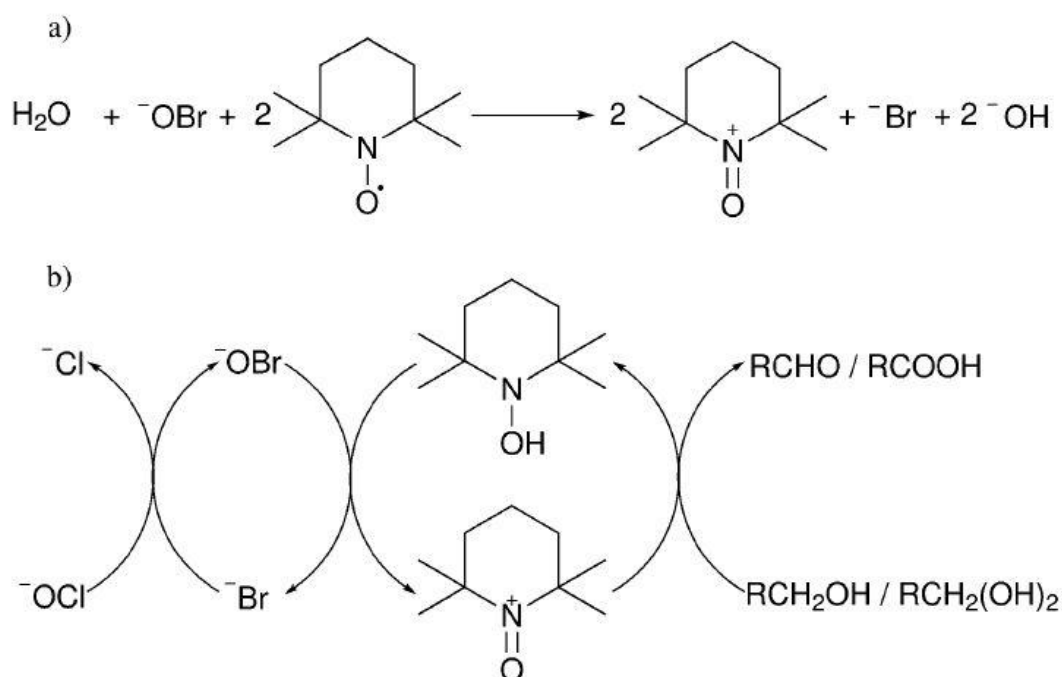


Figure. 3.2 Mechanism of TEMPO mediated oxidation (a) initial formation of oxidant from TEMPO radical and (b) catalytic cycle of TEMPO oxidation.

This converting was carried out by 2, 2, 6, 6-tetramethylpyperidine-1-oxyl (TEMPO) mediated oxidation. In this process TEMPO was used as primary oxidant and sodium hypochlorite was as secondary oxidant. During this process NaBr was used to increase the rate of oxidation through the formation of sodium hypobromite. At pH < 8 the reaction proceeds slowly and selectivity between primary and secondary alcohols was not as prominent as at 9 < pH < 11 where the reaction showed good selectivity to primary alcohol. CCN is better adsorbent over CNC due to the presence of carboxyl group. It may act as better nanofiller in nanocomposite.

3.3 Synthesis of Nano Composite

For the synthesis of nanocomposite, CCN and acrylated Fe₃O₄ (3D crosslinker) were sonicated so that the aggregated particles apart from each other. The mixing procedure was carried out with in sonicator in an ice bath below 20 °C. The mixture of CCN and 3D crosslinker was sonicated long time and that time acrylic acid was added because the dispersion of acrylic acid was occurred homogenously.

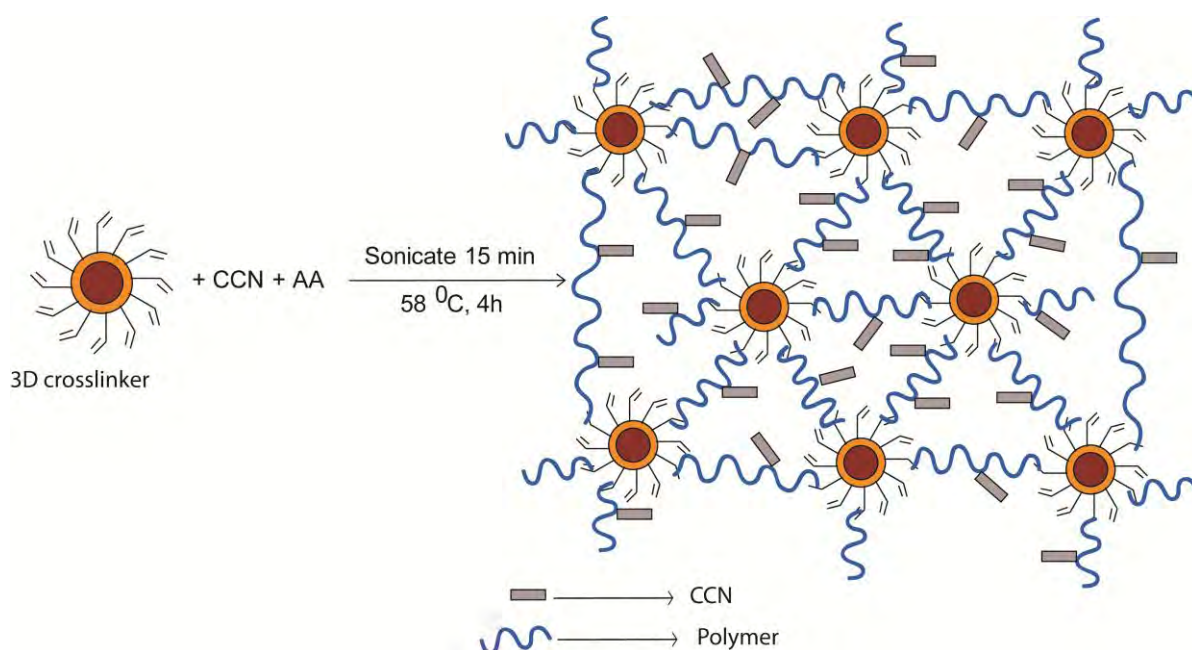


Figure. 3.3 Schematic representation of nanocomposite synthesis

During sonication dissolved potassium per sulfate (KPS) which was used as initiator, was added rapidly so that polymerization undergoes very rapidly. Highly reactive sites of 3D crosslinker are able to link with many more polymer chains. As a result, composite became very sticky and adhesive. When this type of composite was used as adsorbent, they were settled down and adsorption was not much significant. So their adhesiveness needs to decrease and increase the dispersiveness. CCN was used to decrease the adhesive property of the composite materials and increase the dispersive property. At higher amount of CCN and lower amount of 3D crosslinker produced composite was dispersive but not magnetic and the reverse the composite was highly adhesive. After optimize we take the ratio of CCN, 3D crosslinker and acrylic acid was taken 1: 0.4: 30. Then we get proper composite. The composite was dispersive and showed magnetic property. This composite was powder like. After This Reaction We get that for this composite there was no impact of acrylic acid in low or high amount. The best condition of the synthesis of nanocomposite was 58 °C.

3.4 Functional group analysis using FTIR

FTIR measurement were carried out in order to confirm the presence of functional groups on the surface of Fe_3O_4 , Silica coated Fe_3O_4 , Amilated Fe_3O_4 , Acrylated Fe_3O_4 , CCN And Composite.

Table 3.1 Characteristic IR bands of CNC, CCN and nanocomposite

Wavenumber (cm ⁻¹)	Interpretation
2905	C-H stretching
2360	sp ³ C-H stretching
1634	for water adsorption from air by cellulose materials
1422	C-H bending
1377	C-H bending
1317	CH ₂ wagging
1245	C-O out of plane stretching
1110	C-O-C glycosidic ether band
1054	C-O-C pyranose ring stretching vibration
898	-CH ₂ bending

The FTIR spectra of magnetic iron oxide nanoparticles (Fe₃O₄) and modified Fe₃O₄. The 1st one is for Fe₃O₄. The strong absorption peak at 578 cm⁻¹ attribute to the vibration of Fe-O bond and this is the characteristic peak of bare Fe₃O₄. This also indicates the M_{tetrahedral} resonance with oxygen. The peak at 1627 cm⁻¹ indicates the presence of O-H vibration in H₂O and the peak at 3425 cm⁻¹ is attributed to the stretching vibrations of OH adsorbed on the surface of the Fe₃O₄ nanoparticle. The 2nd one is for silica coated Fe₃O₄. The strong peaks at 1080 cm⁻¹ and 804 cm⁻¹ have been assigned to the asymmetric and symmetric linear stretching vibrations of Si-O-Si bonding. The bending vibration absorption peaks of Si-O-Si and Si-OH were observed at 461 cm⁻¹ and 962 cm⁻¹ respectively. These indicates that the successfully coating of silica layer on the surface of magnetic iron oxide nanoparticles.

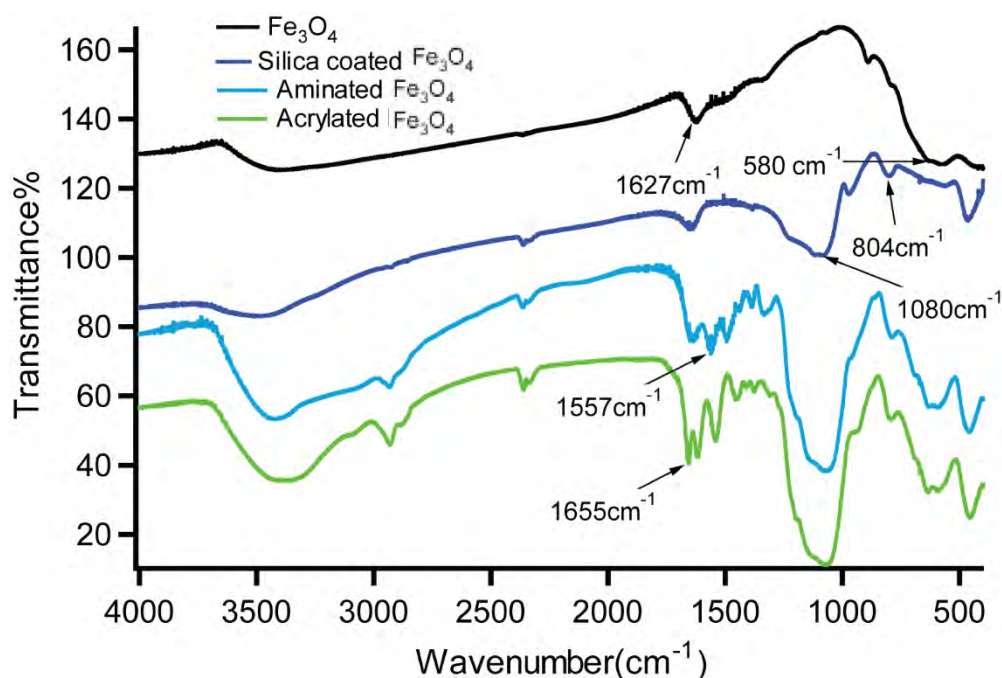


Figure 3.4 FTIR spectra of Fe_3O_4 , silica coated Fe_3O_4 , aminated Fe_3O_4 and acrylated Fe_3O_4

In the spectrum of aminated MION, the two bands at 3422 cm^{-1} and 1650 cm^{-1} can be referred to the N-H stretching vibration and NH_2 bending mode of free NH_2 group, respectively [5]. The anti symmetric C-H stretching vibrations appeared at 2935 cm^{-1} , and the bending vibration absorption peaks of $-\text{CH}_2$ and $-\text{CH}_3$ appeared in 1492 cm^{-1} and 1385 cm^{-1} , respectively; The C-N stretching vibrations appeared at 1335 cm^{-1} . The deformation vibration absorption peak of N-H appeared at 1553 cm^{-1} . These indicate the successful introduction of APTES to the surface of silica coated magnetic NPs. The 4th one is for acrylated Fe_3O_4 . The sharp peak at 1655 cm^{-1} is the characteristic peak of C=C bond. From this it may say that the vinyl group was successfully added to the aminated Fe_3O_4 .

The Figure of below the spectra of First one is for CNC, the second one for CCN, and third one for nanocomposite. The broad peak between 3600 cm^{-1} and 3400 cm^{-1} in the spectra both of CNC & CCN is due to the presence of O-H stretching vibrations. $850\text{--}1500\text{ cm}^{-1}$ region is sensitive to crystal structure of the cellulosic material. Spectral bands at $1420\text{--}1430\text{ cm}^{-1}$ and $893\text{--}897\text{ cm}^{-1}$ are very important to elucidate to the crystal structure of cellulosic material [1]. The peaks at 1163 and 1070 cm^{-1} are related

to the saccharides structure [2] and the peak at 1250 cm^{-1} asymmetrical S=O vibration which shows the presence of sulfate ester groups on the surface of CNC [3]. Other characteristic peaks of CNC that are found in our study are shown in table 3.1.

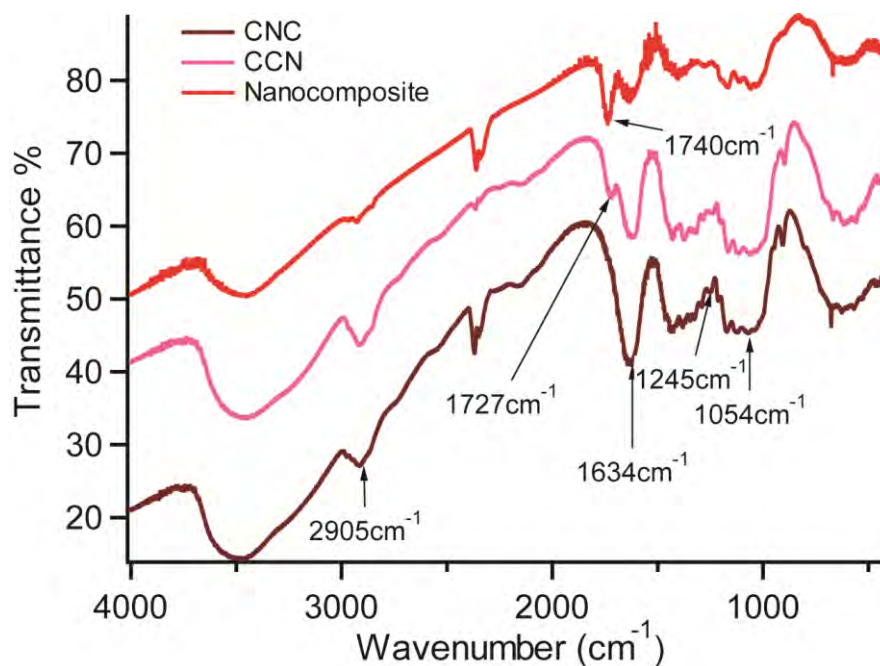


Figure .3.5 FTIR spectra of CNC, CCN and nanocomposite

The second peak is for carboxylated CNC. The FTIR spectrum of the CCN was compared with the spectra of CNC, where the appearance of a new peak at 1728 cm^{-1} corresponds to the carboxyl group, which validates the oxidation process [4]. The 3rd one is for nanocomposite. Here is found a new peak at 1740 cm^{-1} which is for C=O group.

3.5 X-ray photoelectron spectroscopy (XPS)

In order to assess and confirm the bonds that were formed in aminated Fe_3O_4 , acrylated Fe_3O_4 and nanocomposite, were characterized by X-ray photoelectron spectroscopy.

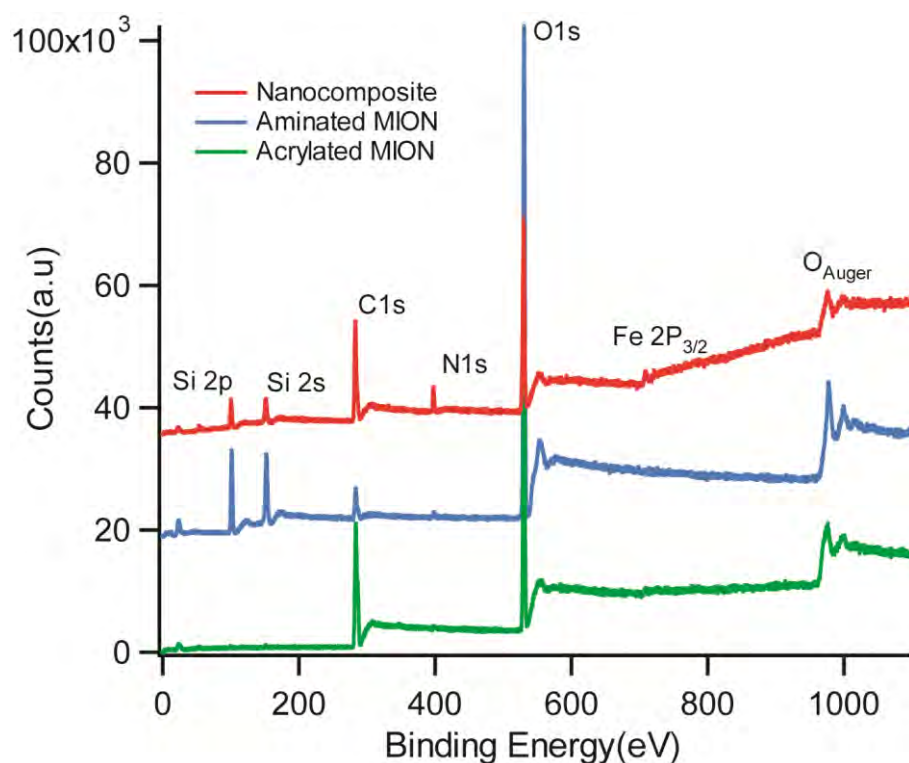


Figure 3.6 Widescan spectra of aminated Fe_3O_4 , acrylated Fe_3O_4 and nanocomposite

The widescan XPS spectra of aminated Fe_3O_4 , acrylated Fe_3O_4 and nanocomposite is shown in Figure 3.6. Widescan spectra give idea about the elemental composition present on the surface. But their bonding nature could not be known by this spectrum. From the Figure 3.6 the widescan spectra of all the samples are similar because there is no elemental change occurred during acrylation or in the formation of nanocomposite. All XPS spectra reveal the presence of C1s, O1s, N1s, Si2s, Si2p. The spectrum of aminated Fe_3O_4 ascribe the dominant species are O and Si. But in case of aminated Fe_3O_4 and nanocomposite the dominant species are O and C. the intensity of N1s very small in aminated and acrylated Fe_3O_4 but significant in nanocomposite. The predominating species C and O are found at the binding energy 283.6 eV and ~ 532.8 eV, respectively. The presence of nitrogen on the surface was detected from its characteristic emission peak at ~ 400 eV and is due to the amination of silica coated Fe_3O_4 and amide formation in acrylated Fe_3O_4 and also in nanocomposite. The binding energy at 100.4 eV and 151.2 eV reveals the existence of silicon on the surface as the

magnetic iron oxide nanoparticles were coated with silica. All the three spectra have a common oxygen auger electron spectrum at binding energy 978 eV.

3.5.1 High Resolution C1s Spectra

Wide scan spectra showed the presence of C but the relation of C with other elements could not explain. For this high resolution of C1s spectra were taken. By this spectrum it is possible to know how the C bonded with other elements. High resolution C1s spectra of aminated Fe_3O_4 , acrylated Fe_3O_4 and nanocomposite are shown in figure 3.7. The C1s peak of aminated Fe_3O_4 can be deconvoluted into three components peak. According to the binding energy these peaks are assigned to the carbon of C-Si (284.3 eV), C-C (285.3 eV) and C-N (285.8 eV) [6-8, 9]. The binding energy 284.5eV corresponds to a carbon atom bound only to silicon atom. C-Si bond found due to the reaction between silanol groups of silica coated MION and 3-aminopropyltetraethylorthosilicate. Binding energy 285.3 ascribes to a carbon atom bound only to other carbon atoms and/or hydrogen atoms. 285.8eV corresponds to a carbon bound to single nitrogen atom. This is due to the terminal amino group linked with methylene group. After acrylation, there is significant changes appeared at the peak position and therefore now the peaks can be deconvoluted into six components which are assigned to C-Si (284.3 eV), C=C (284.6 eV), C-C (285.4 eV), N-C=O (286.6 eV), C=O (288 eV) and O-C=O (289.3 eV) [10, 11]. An additional peak found at 284.6eV compare to aminated Fe_3O_4 which ascribes the presence of C=C and it is the proof of the acrylation of the aminated Fe_3O_4 . Another evidence for this is to the binding energy at 286.6eV for N-C=O which is mainly for the amide formation. The binding energy 289.3eV is due to the presence of O-C=O. This is most probably due to the presence of unreacted methacrylic anhydride. In nanocomposite C1s peak can be deconvoluted into six components peak. The C1s spectrum of nanocomposite shows changing peak position and also peak intensity. With the increasing of binding energy these peaks are assigned to C-Si (284.3 eV), C-C (285.3 eV), C-N (285.8 eV), C-O (286.5 eV), C=O (288 eV), O-C=O (289.3 eV). The peak intensity of C-C is larger compare to another peak. This indicates that the nanocomposite contains greatest C-H or methylene group. The binding energy 286.5eV represents the C-O-C or C-OH bond. This is due to the pyranose ring or alcohol group of the carboxylated

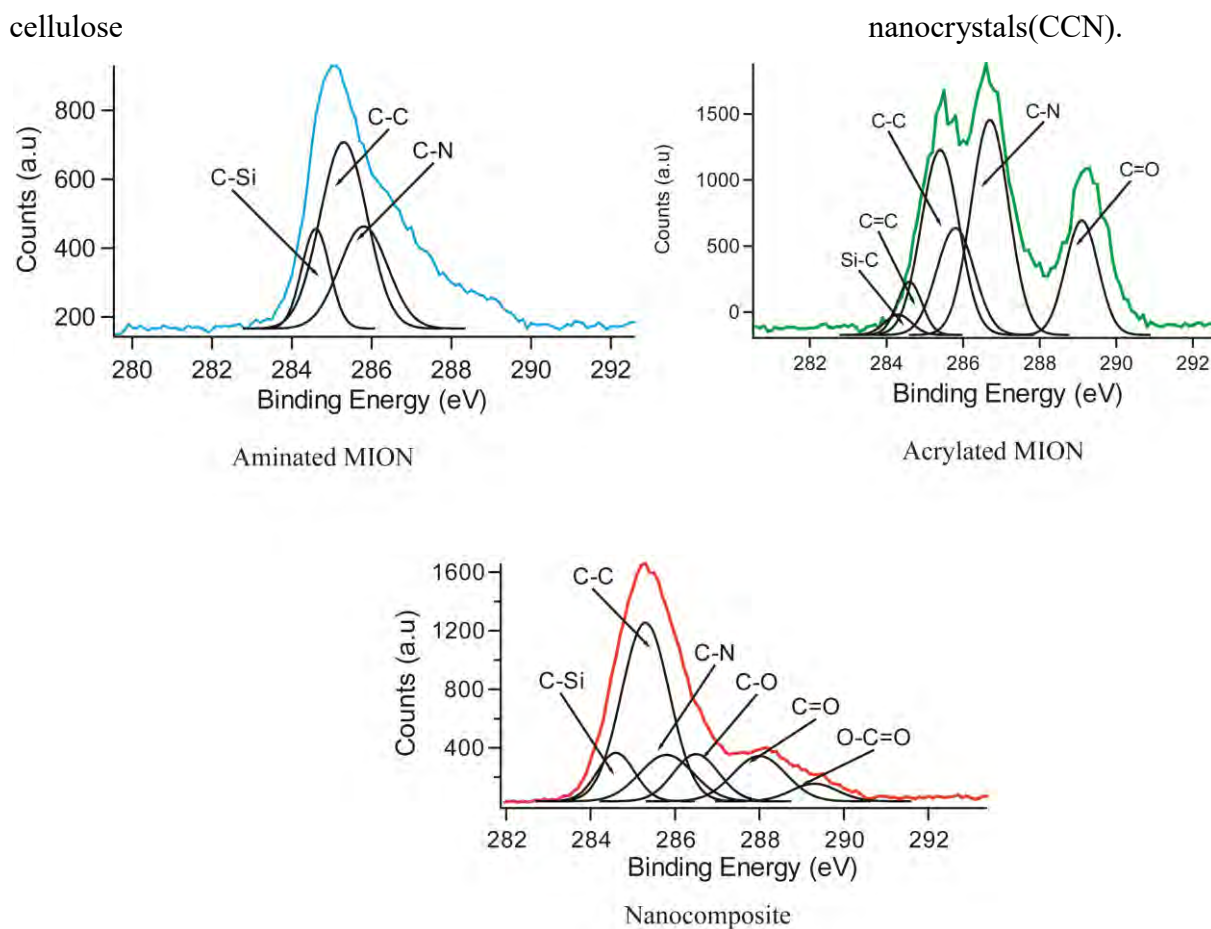


Figure 3.7 High resolution of C1s spectra of aminated Fe_3O_4 , acrylated Fe_3O_4 and nanocomposite

Peak position at binding energy 289.3 eV may indicate the presence of carboxylate ion. This is most probably for the poly(acrylic acid) or CCN.

3.5.2 High Resolution N1s Spectra

From the widescan spectrum it was seen that N was present but the bonding nature of N with other elements was unknown. The bonding nature of N with other elements high resolution of N1s spectra were carried out. The high resolution N1s spectra of aminated Fe_3O_4 , acrylated Fe_3O_4 and nanocomposite are shown in Fig. 3.8.

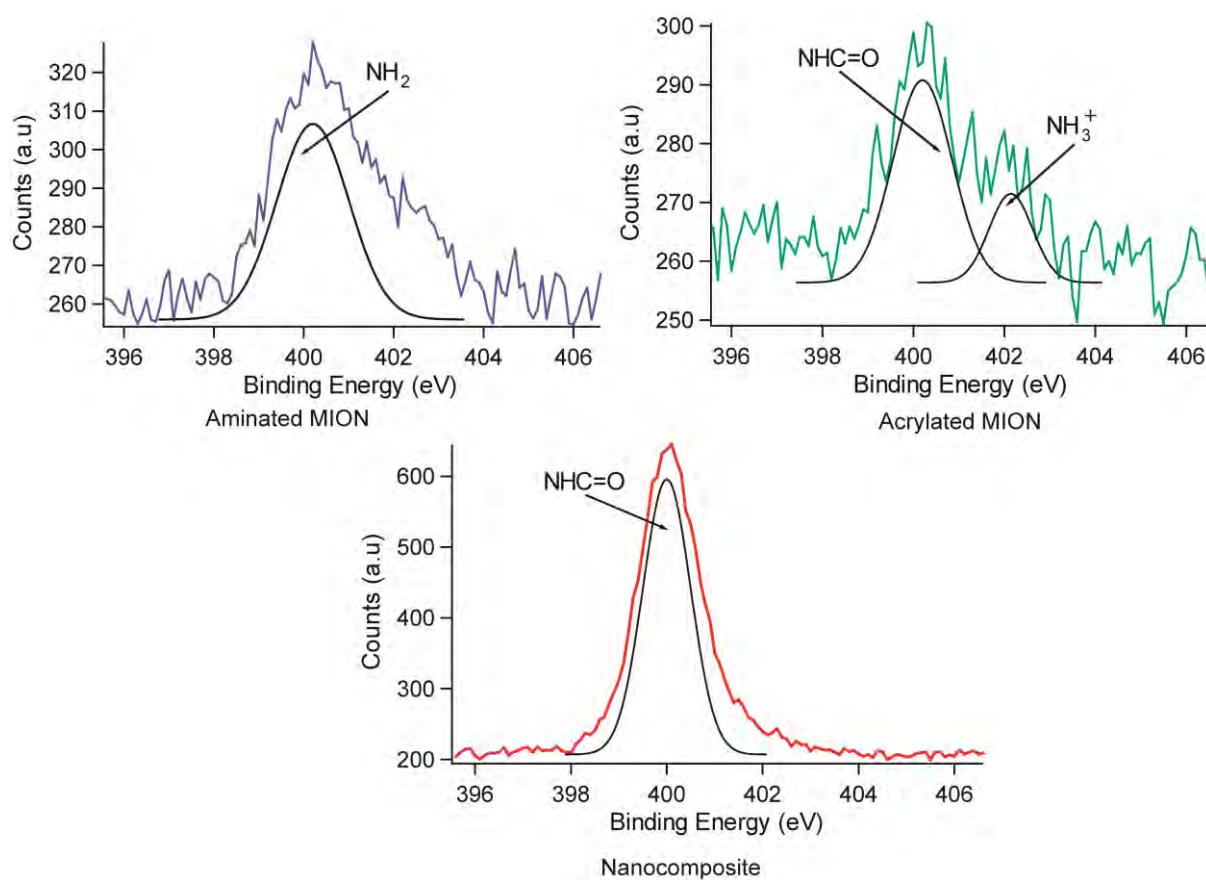


Figure 3.8 High resolution of N1s spectra of aminated Fe_3O_4 , acrylated Fe_3O_4 and nanocomposite

In the case of aminated Fe_3O_4 , there appears one peak at binding energy 400 eV which describes the presence of primary amine at the end of chain. But in the spectra of acrylated Fe_3O_4 there are two deconvoluted peaks appeared. First one is at binding energy 400 eV and second one is for 402 eV. Binding energy 400 eV is attributed to a nitrogen atom linked to a carbon atom by a single bond (amide bond) [12], and the second peak at 402 eV is assigned to the protonated amino group $-\text{NH}_3^+$ [13]. This indicates that all the amino groups in the aminated Fe_3O_4 are not converted to amide. But in the case of nanocomposite there is one peak appeared at 400 eV and indicates the amide group. The protonated amino group which is found in the acrylated Fe_3O_4 may be suppressed by the CCN so for it is disappeared in the nanocomposite.

3.6 Surface morphology study using field emission scanning electron microscope (FE-SEM)

Surface morphology of synthesized CCN, magnetic iron oxide nanoparticles (Fe_3O_4), acrylated Fe_3O_4 and nanocomposite was studied by FE-SEM.

FE-SEM image of magnetic iron oxide nanoparticle is shown in figure 3.9

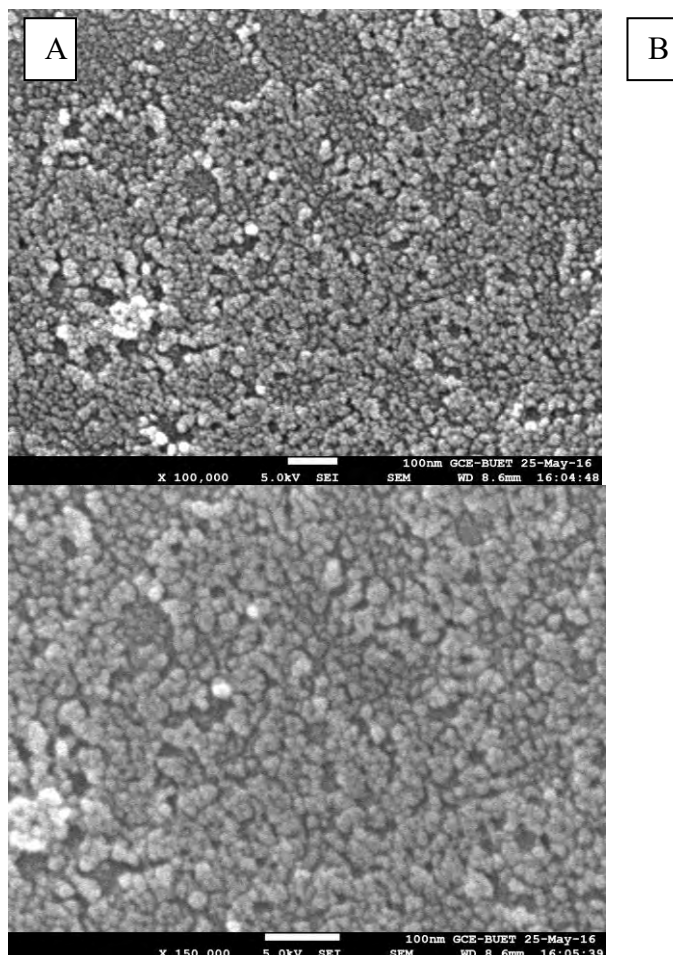
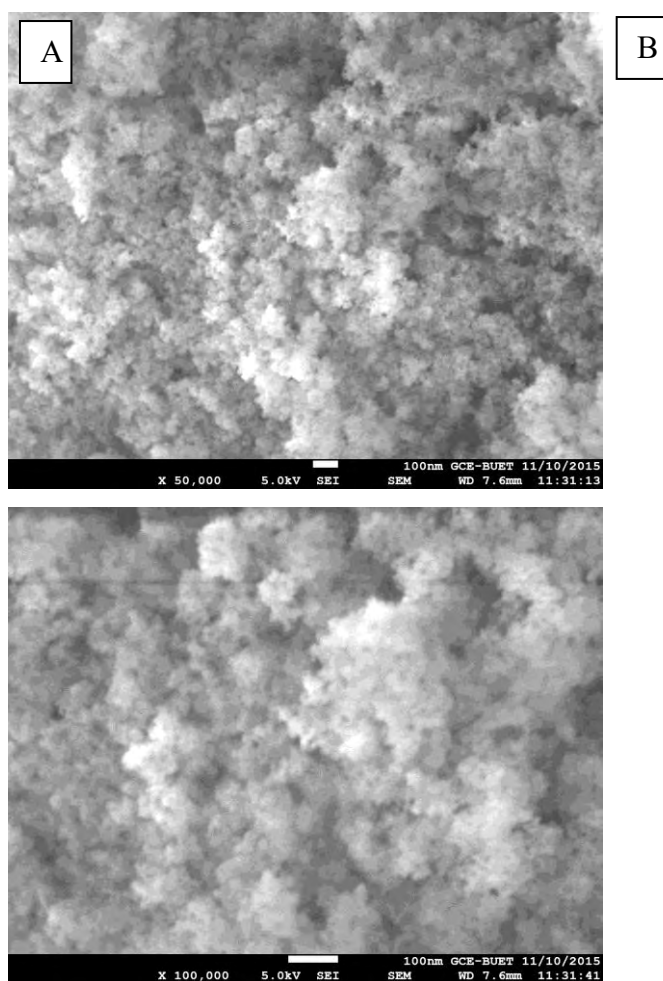


Figure 3.9 FE-SEM image of magnetic iron oxide nanoparticle (Fe_3O_4) (A) Resolution x 100,000 (B) Resolution x 150,000.

From figure 3.14 it is seen that particles of Fe_3O_4 are spherical in shape and highly uniform in size. The average particle size is about 10-15nm. Some particles are very small and about 3-5 nm and some particles aggregate due to large surface area and also magnetic attraction among them. From high resolution image it is clearly seen that particles are finely arranged.

FE-SEM image of silica coated Fe_3O_4 is shown in the figure 3.10.



**Figure 3.10 FE-SEM image of silica coated Fe₃O₄ (A) Resolution x 50,000
(B) Resolution x 100,000.**

From the figure 3.10 it is seen that the average size of the silica coated Fe₃O₄ is about 15-20 nm.

Surface morphology of acrylated Fe₃O₄ was characterized by FE-SEM and the image is shown in figure 3.11.

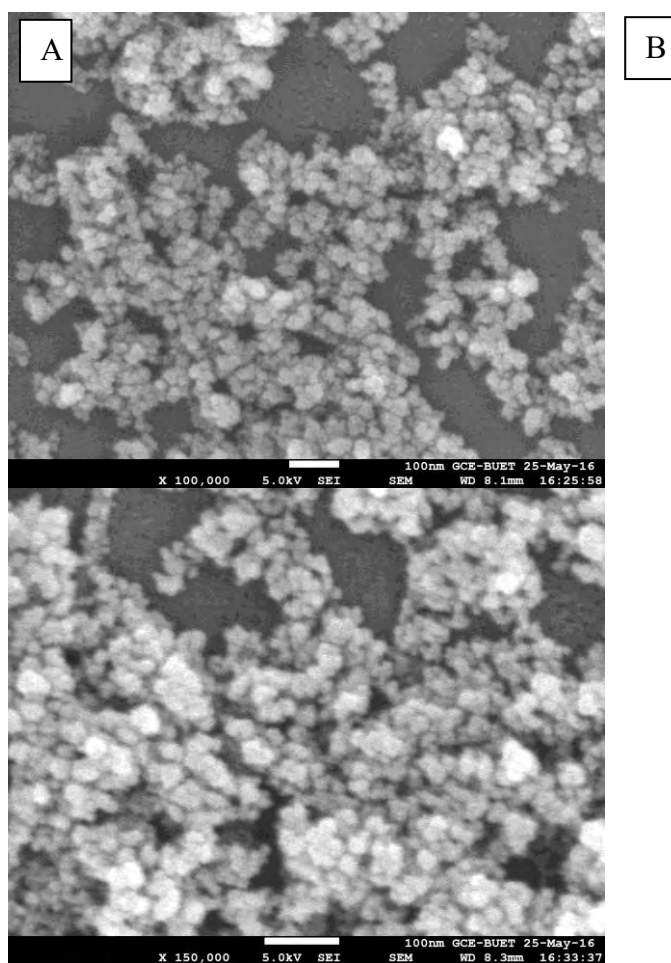


Figure 3.11 FE-SEM image of acrylated Fe₃O₄ (A) Resolution x 100,000 (B) Resolution x 150,000.

From the figure 3.11 it is seen that particles of acrylated Fe₃O₄ are cubic in shape and size is about 20-30nm. Particles are in randomly arranged and also seen that they are on one another. The shape of the particles is all most similar which are seen from the high resolution image.

FE-SEM image of CCN is shown in the figure 3.12.

From the figure 3.12 it is seen that FE-SEM image of CCN is little bit different. The surface is rough and CCNs are randomly arranged. Both low and high resolution images show some white spot.

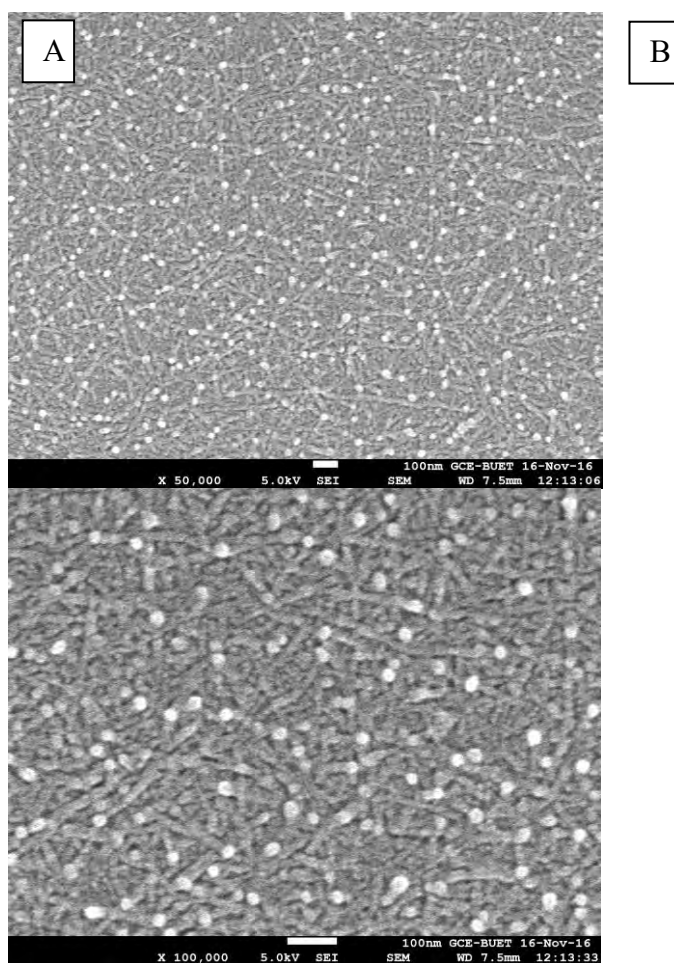
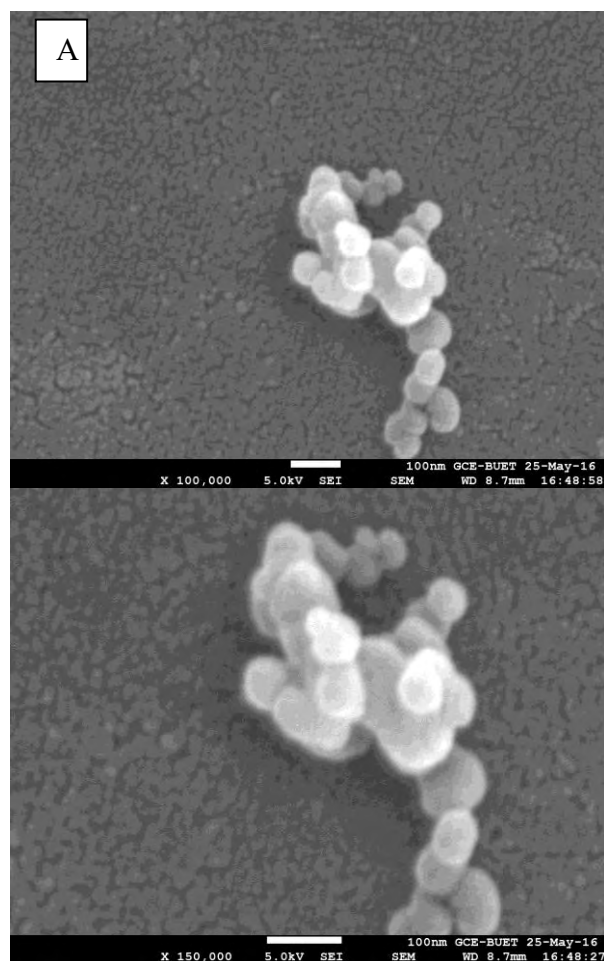


Figure 3.12 FE-SEM image of CCN (A) Resolution x 50,000 (B) Resolution x 100,000.

It is actually spherical CCN which is formed due to concentration variation of TEMPO and sodium hypochlorite. The length of the CCN is about 60-90nm and diameter is approximately 10-20nm. It is also seen that after TEMPO mediated oxidation, the crystal size is little reduced

FE-SEM image of nanocomposite is shown in figure 3.13.



**Figure 3.13 FE-SEM image of nanocomposite (A) Resolution x 100,000
(B) Resolution x 150,000**

Figure 3.13 shows that the particles of nanocomposite are spherical and the diameter is about 60-80nm. The particles are on one another.

3.7 Energy dispersive x-ray (EDX) spectral analysis

Elemental analyses of the CNC, CCN, Fe₃O₄, silica coated Fe₃O₄, acrylated Fe₃O₄ and nanocomposite have been performed by Energy Dispersive X-ray (EDX) method. The EDX patterns are presented in Figure 3.18-3.20. The peaks observed at 0.277, 0.392, 0.525, 1.739 and 6.398 keV, for K lines of C, N, O, Si and Fe respectively. The percentages of Fe, O, Si, N, and C were determined from the intensity of the lines and are summarized in Table 3.2.

Table 3.2 Elemental composition of magnetic and cellulosic compound

Sample	Iron (Fe) %	Oxygen (O) %	Silicon (Si)%	Nitrogen (N)%	Carbon (C)%
Fe ₃ O ₄	31	69	×	×	×
Silica coated Fe ₃ O ₄	13	42	43	×	×
Acrylated Fe ₃ O ₄	25	40	12	4	19
CNC	×	52	×	×	47
CCN	×	56	×	×	44
Nanocomposite	1	56	31	1	11

From the table it is seen that iron content 31% and oxygen content 69%. It is approximately equal to the theoretical value of Fe₃O₄. In case of CNC, there is some sulfur as the acid hydrolysis was carried out by sulfuric acid and it may form sulfate ester group.

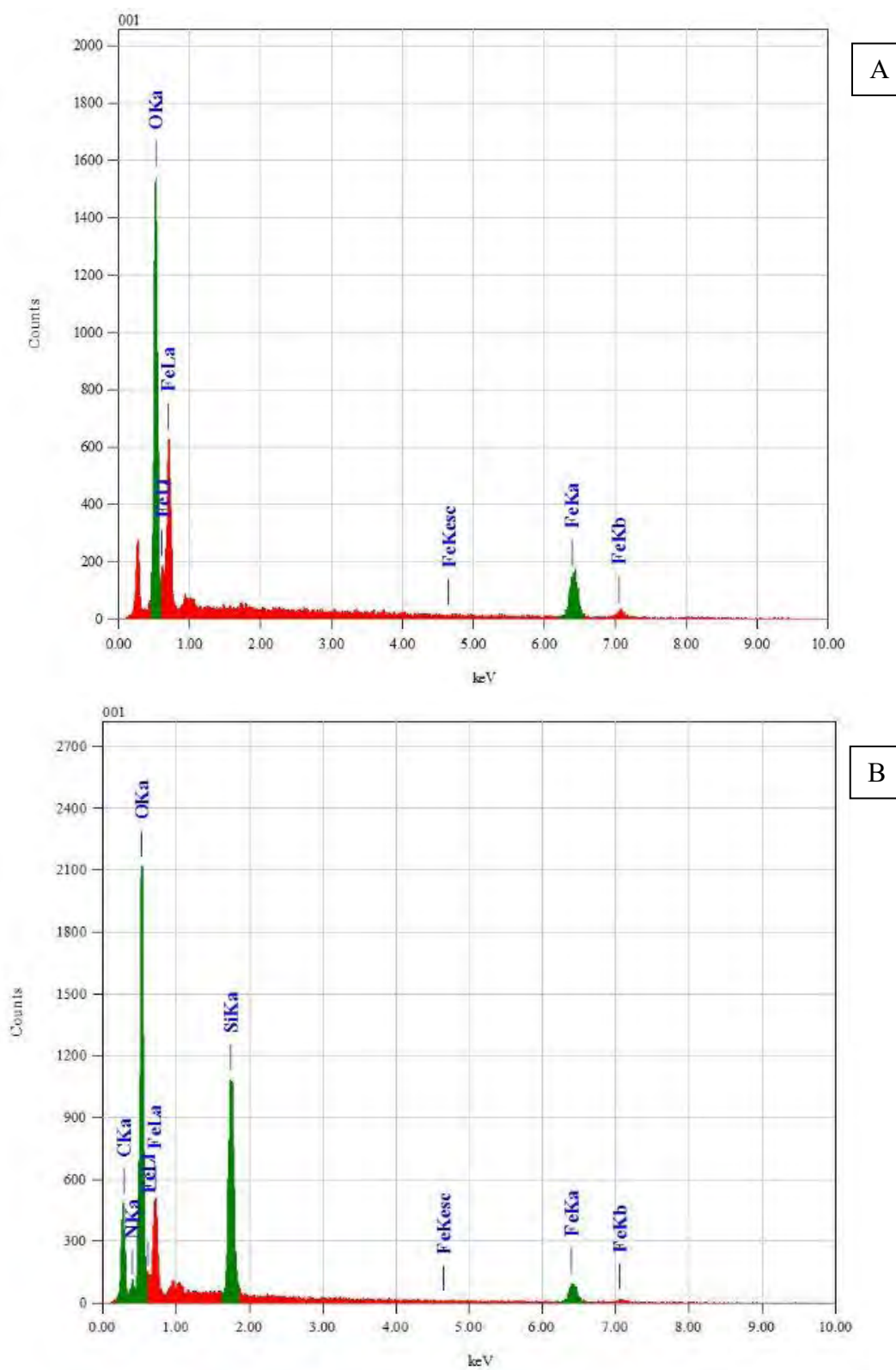


Figure 3.14 EDX spectra of (A) Fe₃O₄ and (B) silica coated Fe₃O₄

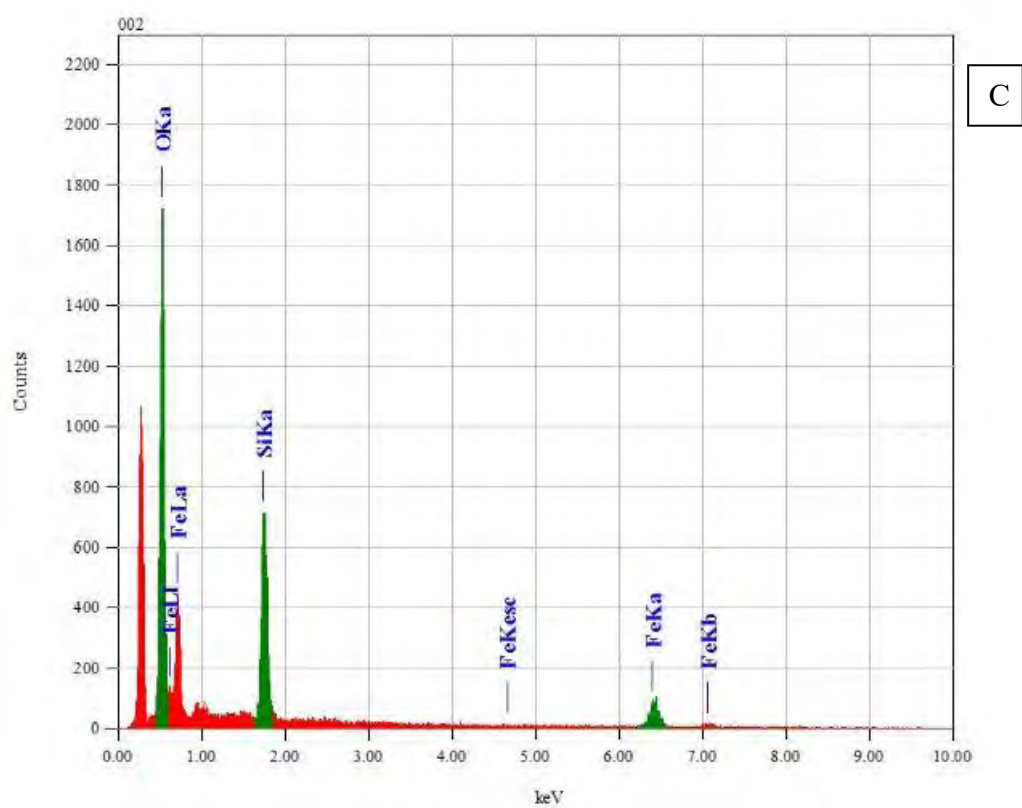


Figure 3.16 EDX spectra of (C) acrylated (Fe_3O_4)

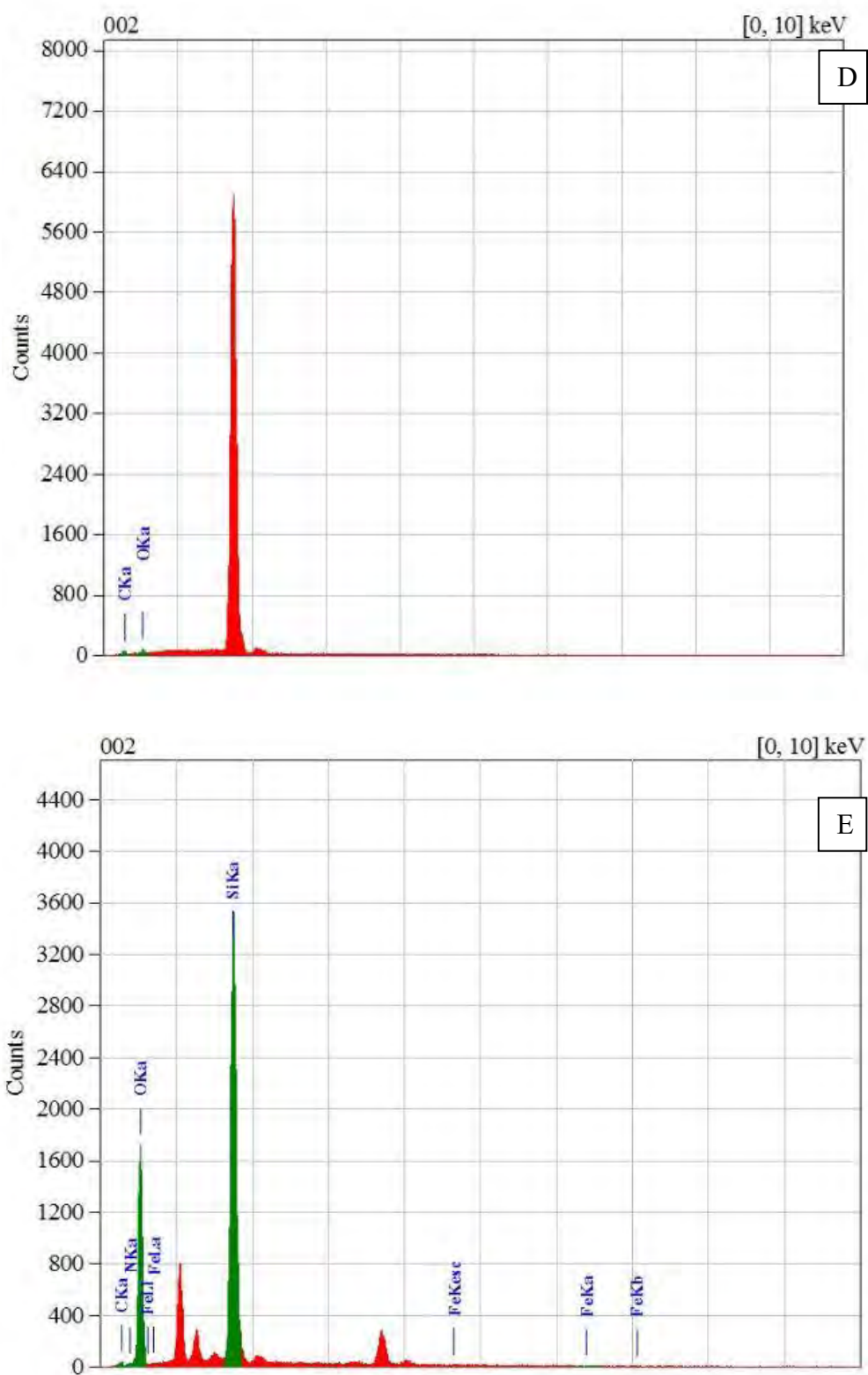


Figure 3.17 EDX spectra of (D) CCN and (E) nanocomposite

3.8 Thermogravimetric analysis

Thermal analysis technique such as thermogravimetric analysis was carried out to measure the thermal stability and pyrolysis behavior of CCN, acrylated Fe_3O_4 , composite without CCN and nanocomposite at the temperature range 20-800 $^{\circ}\text{C}$. The TGA curves of CCN, acrylated Fe_3O_4 , composite without CCN and nanocomposite are shown in figure 3.21.

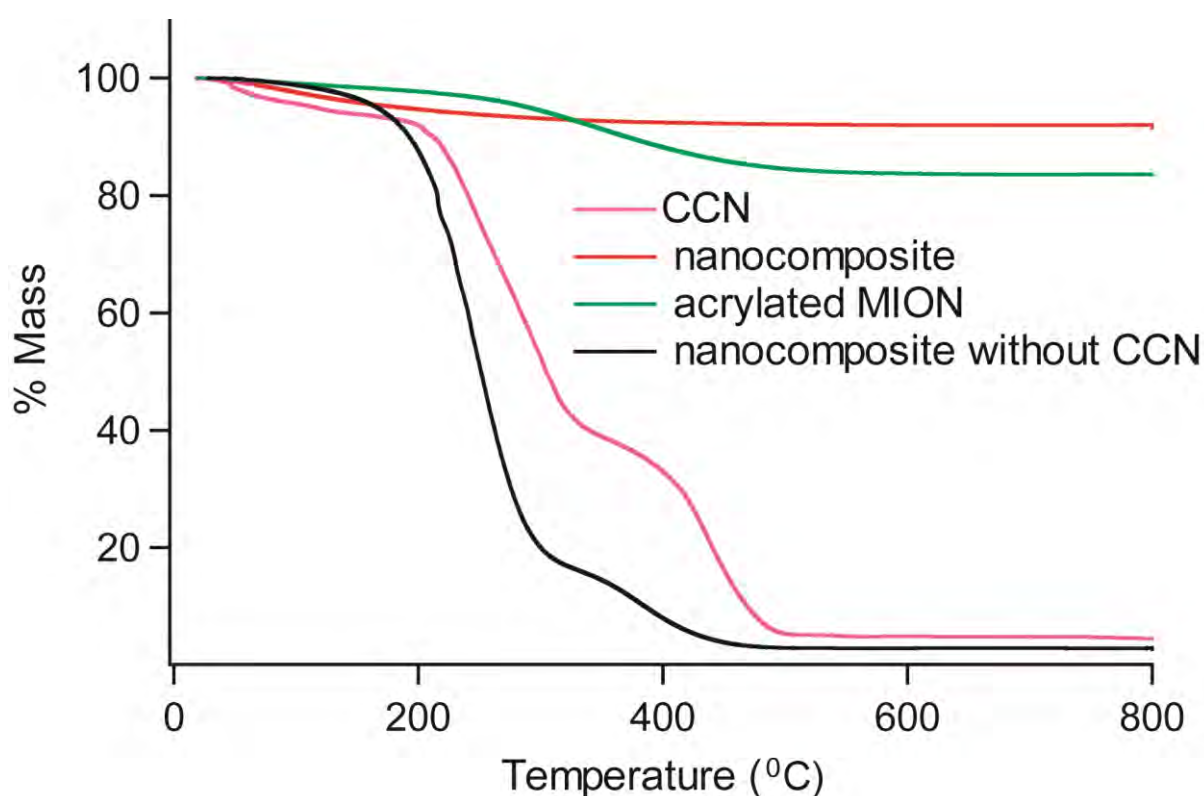


Figure 3.18 TGA curves of CCN, acrylated Fe_3O_4 , composite without CCN and nanocomposite

From the TGA curve, it is seen that all the samples showed a slight weight loss at low temperatures (< 150 $^{\circ}\text{C}$), which is due to the release of water molecules weakly adsorbed on the particles surface. It is also noticed that the degradation behavior was different in the high temperature range. In case of CCN, the initial degradation temperature starts up to 204 $^{\circ}\text{C}$ (8.56%). A drastic change appears up to 330 $^{\circ}\text{C}$ due to oxygen containing groups disappeared and about 59% weight loss occurred. The final degradation temperature of CCN is 406 $^{\circ}\text{C}$. After 400 $^{\circ}\text{C}$ only residue of carbon

remained. In case of acrylated Fe_3O_4 , the initial degradation temperature is 257°C . With the increasing temperature up to 483°C , oxygen containing group degraded and about 15% weight lost. Next the temperature up to 800°C there is slightly weight change appeared because silica and iron remain unchanged at high temperature. In case of composite without CCN (3D crosslinked poly(acrylic) acid), the initial degradation temperature is 185°C . Maximum weight lost occurred at temperature 297°C which is attributed to the decomposition of the crosslinked polymer network. About 80% weight lost occurred at this temperature. Next weight lost attributed to the oxygen containing groups disappeared. This composite is thermally less stable compared to CCN and acrylated Fe_3O_4 . But in the case of nanocomposite, the initial degradation temperature is 216°C . At this stage about 6% weight lost occurred due to the removal of moisture and adsorbed water. Mechanical strength of nanocomposite was increased due to the incorporation of CCN and dramatically changed its thermal sensitivity. Temperature up to 450°C only 2% weight lost happened and after that weight remained almost same. So compare to 3D crosslinked poly(acrylic acid) composite and corresponding components, we can say the synthesized nanocomposite is highly thermo stable.

3.9 Magnetic property analysis

The superparamagnetic behavior of Fe_3O_4 , Acrylated Fe_3O_4 (3D crosslinker) and PAA/3D/CCN (PAAMCCN) were measured by plotting magnetization curves. The hysteresis loops of Fe_3O_4 , Acrylated Fe_3O_4 (3D crosslinker) and PAA/3D/CCN (PAAMCCN) are shown in Figure 3.19 it can be seen that the magnetic saturation values of these are about 22, 20.5 and 7.5 emu/g respectively.

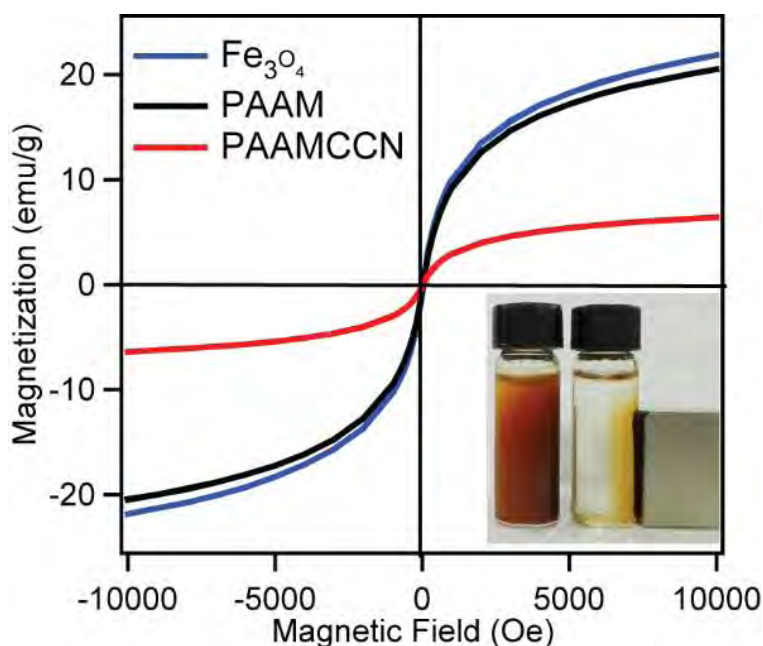


Figure 3.19 Magnetic hysteresis loop of Fe_3O_4 , Acrylated Fe_3O_4 and PAA/ Fe_3O_4 /CCN (PAAMCCN) composite. The inset photograph: separation of PAA/ Fe_3O_4 /CCN (PAAMCCN) composite from aqueous dispersion using a magnet bar.

The decrease in magnetic saturation of the PAA/ Fe_3O_4 /CCN (PAAMCCN) composite in comparison with Acrylated Fe_3O_4 (3D crosslinker) may be attributed to the increased mass of the Functionalization amine group, acrylated group and polymer. Despite Even though the extra weight of PAA/ Fe_3O_4 /CCN (PAAMCCN) composite it exhibit the paramagnetic behavior. The inset photograph shows the magnetic behavior of PAA/ Fe_3O_4 /CCN (PAAMCCN) composite and it can easily separate from aqueous solution using an external magnet.

3.10 Dye (Methylene blue) removal experiment.

3.10.1 Adsorption Test

The adsorption capacity of Methylene Blue on Acrylated Fe_3O_4 and PAA/ Fe_3O_4 /CCN (PAAMCCN) were study in batch process. In first few minutes the adsorption capacity of MB increase vertically with increasing time. The capacity of dye adsorption of Acrylated Fe_3O_4 was lower than PAA/ Fe_3O_4 /CCN (PAAMCCN) according to the adsorption capacity q_t and time t . The figure 3.20 show that the due to dispersive

property of CCN the adsorption capacity of PAA/Fe₃O₄/CCN (PAAMCCN) increasing significantly. For an example

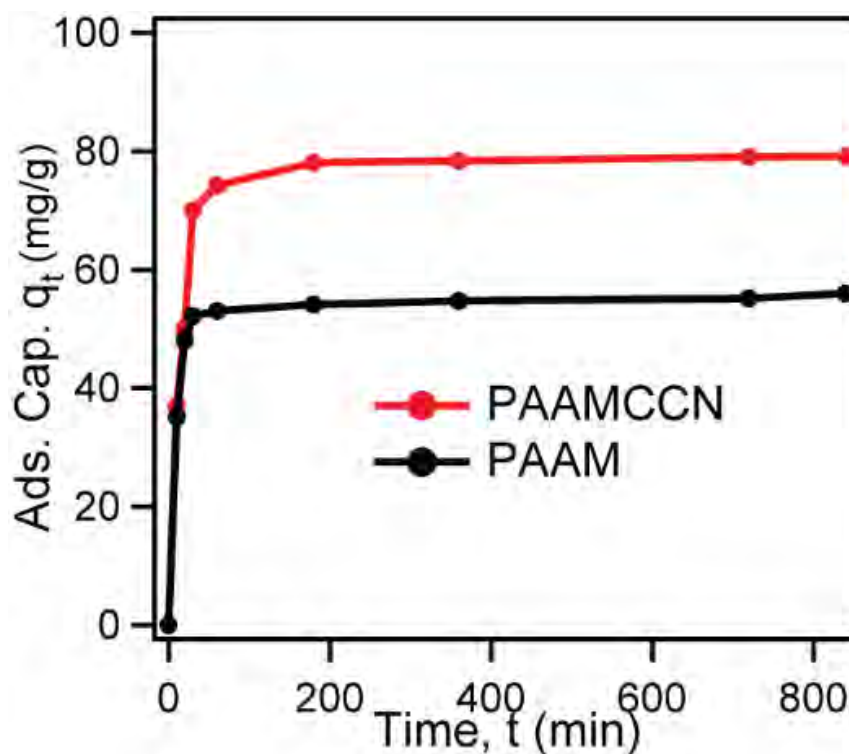


Figure. 3.20 Adsorption capacity q_t of MB on Acrylated Fe₃O₄ and PAA/Fe₃O₄/CCN (PAAMCCN) as a function of adsorption time t , with 20 mg/L initial concentration of MB, pH=7.

The adsorption kinetics shows the evolution of the adsorption capacity through time and it is necessary to identify the types of adsorption mechanism in a given system. The following models are used to describe the adsorption kinetics behavior:

3.10.2 Pseudo-first order model

The adsorption kinetics can be described by a pseudo-first order equation

$$\log(q_e - q_t) = \log q_e - \frac{k_1 t}{2.303}$$

Where q_e and q_t (mg/g) represent the amounts of MB adsorbed at equilibrium and at any adsorption time t . k_1 (min^{-1}) are pseudo-first rate constant.

The adsorption rate constant k_1 can be experimentally determined by the slope of linear plots $\log(q_e - q_t)$ vs. t

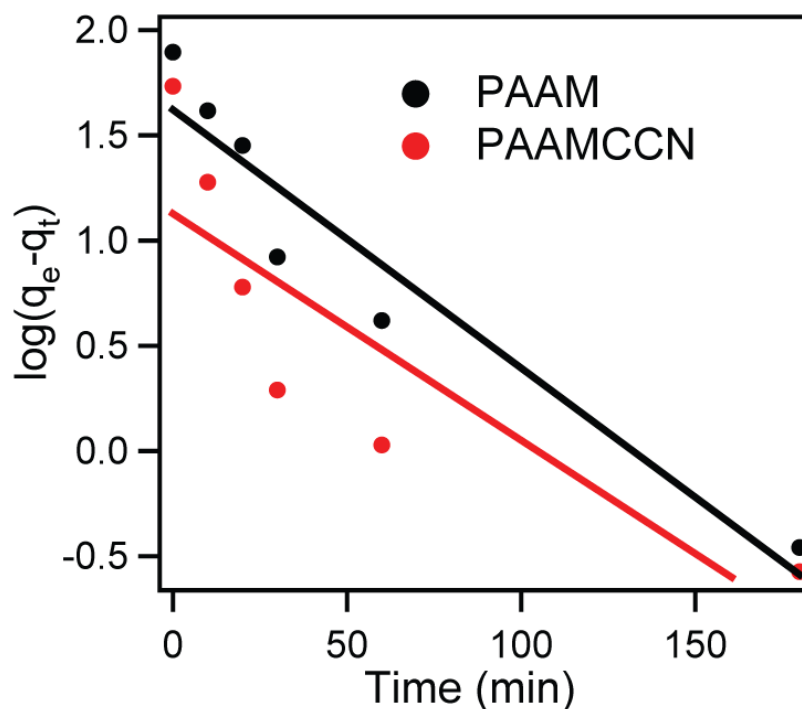


Figure. 3.21 Fitting the adsorption kinetics of MB on PAAM and PAAMCCN using the pseudo-first order kinetic model.

3.10.3 Pseudo-second order model

The adsorption kinetics can be described by a pseudo-first order equation

$$\frac{t}{q_t} = \frac{1}{q_e^2 k_2} + \frac{t}{q_e}$$

Where q_e and q_t (mg/g) represent the amounts of MB adsorbed at equilibrium and at any adsorption time t . k_2 (min^{-1}) are pseudo-first rate constant.

The adsorption rate constant k_2 can be experimentally determined by the slope of linear plots t/q_t vs. t

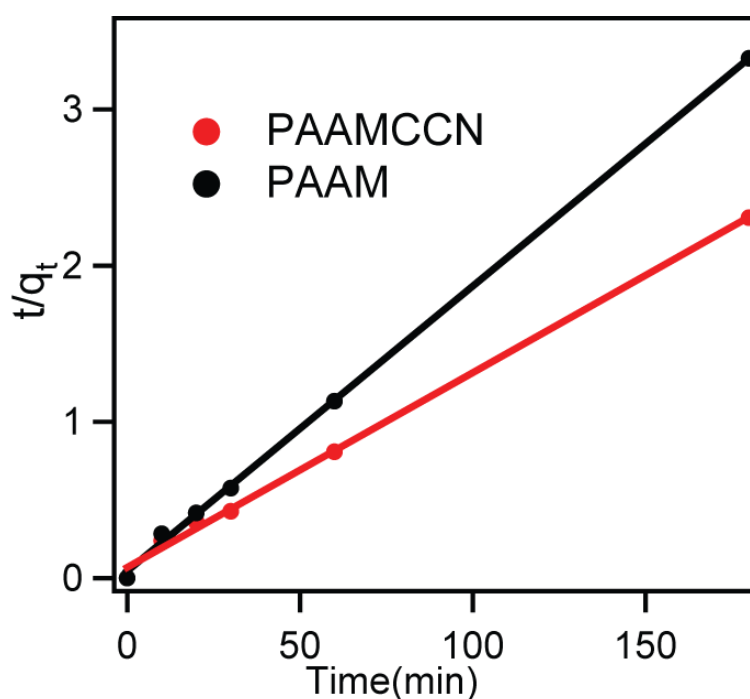


Figure. 3.22 Fitting the adsorption kinetics of MB on PAAM and PAAMCCN using the pseudo-second-order kinetic model.

The pseudo first order kinetic model assumes that the adsorption erate is proportional to the number of adsorption sites. While the pseudo second order kinetic model assumes that the adsorption rate is proportional to the square of available number of adsorption sites²⁰.

Pseudo-first-order

pseudo-

second-order

Adsorbents	q_e (mg/g)	$K_1(\text{min}^{-1})$	q_e cal(mg/g)	R^2	K_2	q_e cal(mg/g)	R^2
PAAM	56.006	0.0018	17.62	0.5402	0.00251	54.854	0.97329
PAAMCCN	79.0662	0.0033	24.124	0.8652	0.000316	80.3212	0.98329

Table: 3.3 Parameters for the fitting of the adsorption of MB on PAAM and PAAMCCN using the pseudo-first-order and pseudo-second-order kinetic models.

Figure 3.21 and 3.22 show the fitting for the adsorption of MB on PAAM and PAAMCCN using the pseudo-first-order kinetics and pseudo-second-order kinetics, respectively. All kinetic parameters obtained by linear regression of the two kinetic models are summarized in Table1. The higher correlation coefficient values (R^2) in Table1 and the good agreement between the measured $q_{e,exp}$ and the calculated $q_{e,cal}$ indicate a better fitting of the data using the pseudo-second-order kinetic model than the pseudo-first-order model for the adsorption behaviors of MB on PAAM and PAAMCCN.

To better understand the interactions between the adsorbents and MB, the adsorption data has been analyzed using Langmuir and Freundlich isotherm models

3.10.4 Langmuir isotherm

Langmuir isotherm equation is

$$\frac{C_e}{q_e} = \frac{1}{bq_m} + \frac{C_e}{q_m}$$

Where, C_e (mg/g) is the equilibrium concentration of the MB. q_m (mg/g) is the maximum Langmuir monolayer adsorption capacity. b is related to the energy of the adsorption [21].

The Langmuir adsorption isotherm assumes that adsorption takes place at specific homogeneous sites within the adsorbent and has found successful application to many sorption processes of monolayer adsorption.

3.10.5 Freundlich isotherm model

Freundlich isotherm equation is

$$\log q_e = \log K_f + \frac{1}{n} \log C_e$$

where K_f and n are the indicators of adsorption capacity and adsorption intensity, respectively, which can be determined from the fitting of experimental data.

The Freundlich isotherm model is an empirical model assuming a heterogeneous surface of adsorbent.

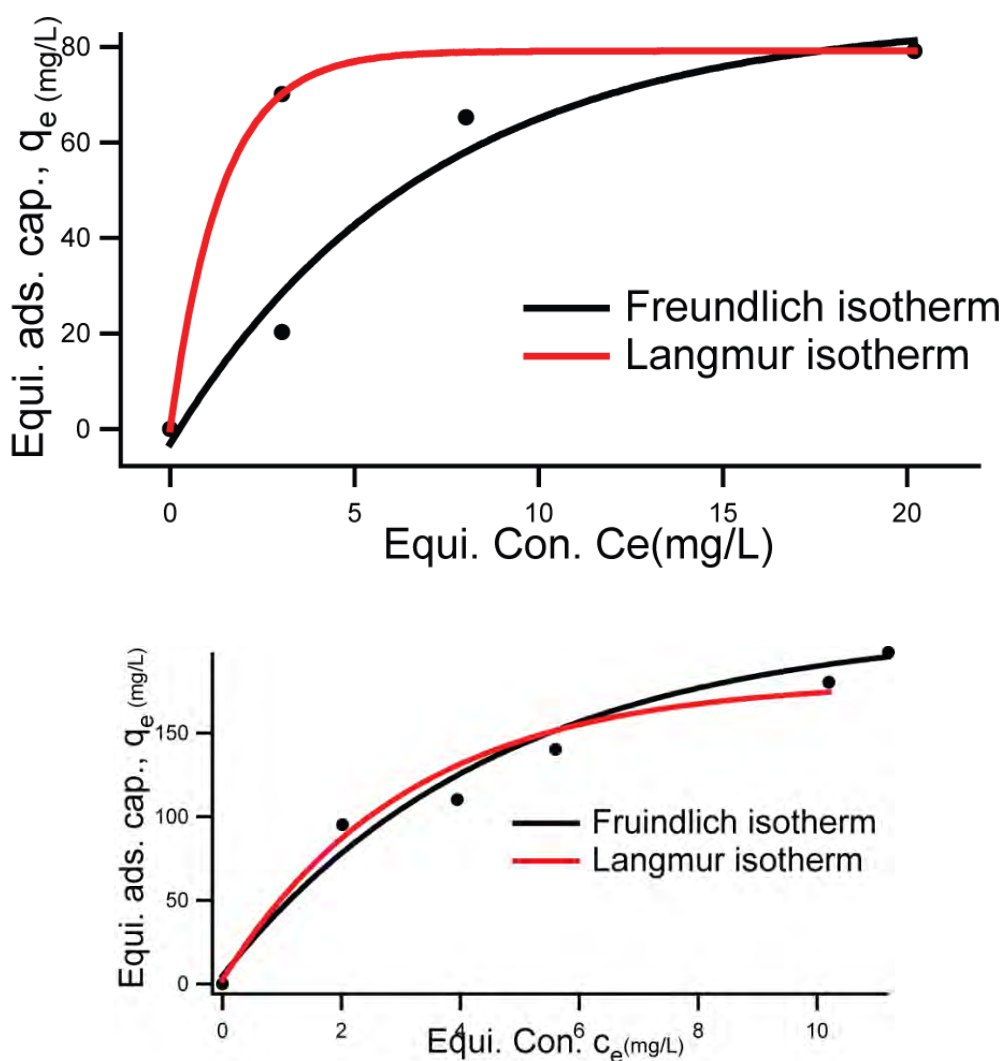


Figure.3.23 Isotherms of the adsorption of MB on (a) PAAM and (b) PAAMCCN, with a contact time of 14 h.

The figure shows the fitting of adsorption data using the Langmuir and Freundlich models for the adsorption of MB on PAAM and PAAMCCN. The regression coefficients (R^2) suggest that the Langmuir model fits the adsorption better, which implies that both PAAM and PAAMCCN likely possess homogeneous adsorption surfaces and the adsorption of MB on these two adsorbents is likely monolayer. However, it should be noted that previous studies have shown that certain heterogeneous materials/surfaces and heterogeneous adsorption could also obey the Langmuir model.

3.10.6 pH effect

The pH of the dye solution plays an important role in the whole adsorption process, particularly on the adsorption capacity. From the adsorption capacity it is noted that PAAMCCN exhibits higher than PAAM over the whole pH range investigated. Because the CCN ensure the dispersiveness of materials. The reactive side increase due to dispersiveness. Methylene Blue carry chloride ion which can deionized in aqueous solution and make a electrostatic attraction with negative charge carboxylic group.

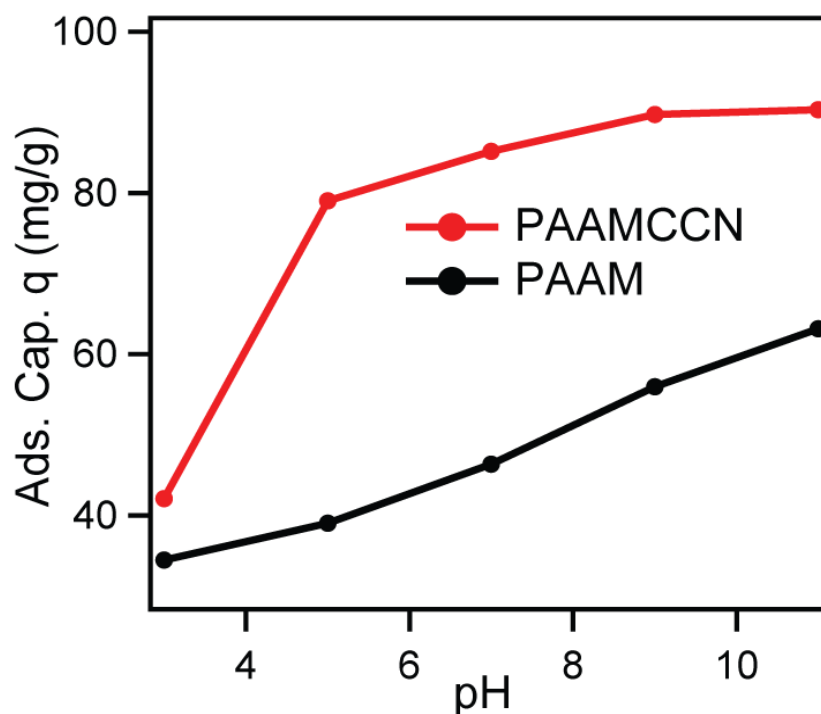


Figure 3.24 Adsorption capacity of MB on PAAM and PAAMCCN under different pH

Our materials PAAMCCN contains two types of carboxylic group One is acrylic acids group and other is cellulose group. As a result of their relatively acidic nature, carboxylic acids will ionize if placed in an environment of adequate basicity. Thus

carboxylic acids (typical pKa values in the range of 3-5) in aqueous media of pH>7, such as methylene blue aqueous solutions, will exist primarily in the ionized, conjugate base form.

3.10.7 Effect of pH on zeta potential

Zeta potential difference existing between the surface of a solid particle immersed in a conducting liquid (e.g. water) and the bulk of the liquid. The zeta potential depends on surface charge density. Increasing pH the zeta potential of both PAAM and PAAMCCN decreases, and the zeta potential of PAAMCCN is lower than that of PAAM over the whole pH range.

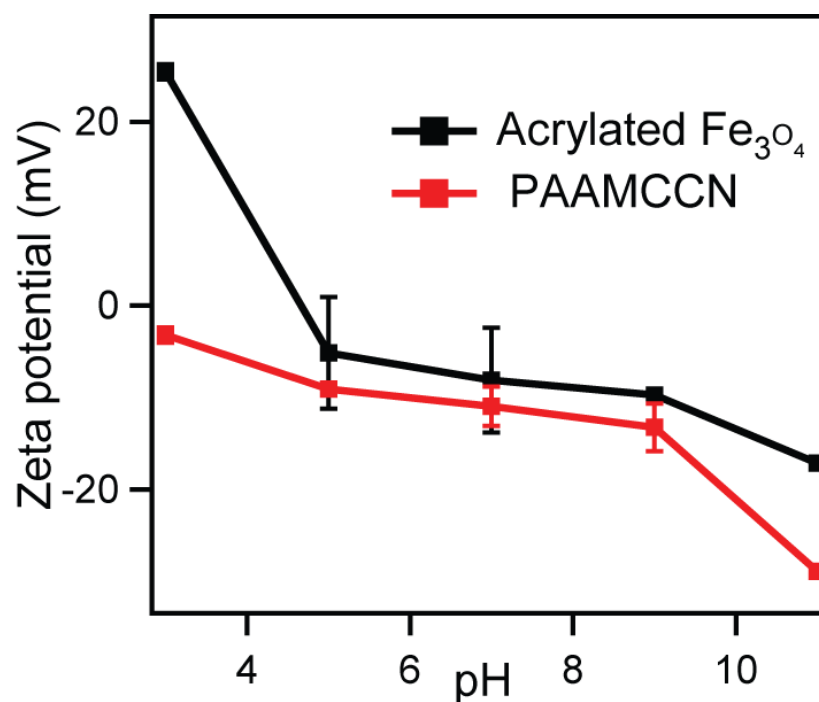


Figure. 3.25 Zeta potential of Acrylated Fe₃O₄ and PAAMCCN

The decreased zeta potential can be attributed to that the carboxylic groups on PAAM and on the PAA chains of PAAMCCN deprotonate as pH increases leading to more negatively charged surfaces.

3.11 Conclusion

In this work focused on liquid phase adsorptive removal of cationic dye. For this purpose we synthesis a magnetic nano composite based on polyacrylic acid carboxylated cellulose nanocrystal. (PAAMCCN) in facile method. The adsorption behaviors of a model dye polutant, methylene blue, on PAAM and PAAMCCN were evaluated in batch tests. The adsorption kinetics could be quite successfully fitted by a pseudo-second order kinetic equation. The Langmuir, Freundlich adsorption isotherm models were used to express the adsorption phenomenon of the methylene blue. The removal capacity of MB by both PAAM and PAAMCCN adsorbents also increases with increasing solution pH, and the zeta potential of both PAAM and PAAMCCN decreases with increasing the solution pH which enhances the electrostatic attraction between MB and the composite surfaces. PAAMCCN also can be easily separated under an external magnetic field with excellent recyclability and reusability. The PAAMCCN nanocomposite has great potential application as a novel adsorbent for the removal of cationic organic pollutants from wastewater.

References:

1. A. Kumar., Y. S. Negi., V. Choudhary., N. K. Bhardwaj., “Characterization of cellulose nanocrystals produced by acid-hydrolysis from sugarcane bagasse as agro-waste”, *J. Mater. Physic. Chem.*, vol. 2 (1), pp. 1-8, (2014).
2. J. P. de Mesquita., C. L. Donnici., F. V. Pereira., “Biobased nanocomposites from layer-by-layer assembly of cellulose nanowhiskers with chitosan”, *Biomacromole.*, vol. 11, pp. 473–480, (2010).
3. J. Gu., J. M. Catchmark., E. Q. Kaiser., D. D. Archibald., “Quantification of cellulose nanowhiskers sulfate esterification levels”, *Carbohydr. Polym.*, vol. 92, pp. 1809–1816, (2013).
4. F. Azzam., L. Heux., J. Putaux., B. Jean., “Preparation by grafting onto, characterization, and properties of thermally responsive polymer-decorated cellulose nanocrystals”, *Biomacromol.*, vol. 11, pp. 3652–3659, (2010).

5. J. Xu., C. Ju., J. Sheng., F. Wang., Q. Zhang., G. Sun., M. Sun., “Synthesis and characterization of magnetic nanoparticles and its application in lipase immobilization”, *Bull. Korean Chem. Soc.*, vol. 34, pp. 8, (2013).
6. J. Diaz., G. Paolicelli., S. Ferrer., F. Comin., “Separation of the sp³ and sp² components in the C1s photoemission spectra of amorphous carbon films” *Phys. Rev. B.*, vol. 54, pp. 8064- 8069, (1996).
7. Q. X. Li., J. Y. Wen., K. G. Neoh., E. T. Kang., D. F. Guo., “Dopamine-induced reduction and functionalization of graphene oxide nanosheets” *Macromole.*, vol. 43, pp. 8336-8339, (2010).
8. H. C. Gao., Y. M. Sun., J. J. Zhou., H. W. Duan., “Mussel-inspired synthesis of polydopamine-functionalized graphene hydrogel as reusable adsorbents for water purification” *Acs Appl. Mater. Interfaces*, vol. 5, pp. 425-432, (2013).
9. M. Y. Bashouti., C. A. Garzuzi., M. de la Mata., J. Arbiol., J. Ristein., H. Haick., S. Christiansen., “Role of Silicon Nanowire Diameter for Alkyl (Chain Lengths C1–C18) Passivation Efficiency through Si–C Bonds”, *Langmuir*, vol. 31, pp. 2430–2437, (2015).
10. F. Liu., F. Sun., Q. Pan., “Highly compressible and stretchable superhydrophobic coating inspired by bio-adhesion of marine mussels” *J. Mater. Chem., A*, vol. 2, pp. 11365-11371, (2014).
11. S. Barazzouk., C. Daneault., “Amino acid and peptide immobilization on oxidized nanocellulose: spectroscopic characterization”, *Nanomaterials*, vol. 2, pp. 187-205, (2012).
12. R. J. J. Jansen., H. Van Bekkum., “XPS of nitrogen-containing functional groups on activated carbon”, *Carbon*, vol. 33, pp. 1021–1027, (1995).
13. Y. Zubavichus., M. Zharnikov., A. Shaporenko., O. Fuchs., L. Weinhardt., C. Heske., E. Umbach., J.D. Denlinger., M. Grunze., “Soft X-ray induced decomposition of phenylalanine and tyrosine: A comparative study”, *J. Phys. Chem. A*, vol. 108, pp. 4557–4565, (2004).
14. Y. P. He., S. Q. Wang., C. R. Li., Y. M. Miao., Z. Y. Wu., B. S. Zou., “Synthesis and characterization of functionalized silica-coated Fe₃O₄ superparamagnetic nanocrystals for biological applications” *J. Phys. D: Appl. Phys.* vol. 38, pp. 1342–1350, (2005).

15. H. Zhang.,X. Zhong., J. J. Xu., H. Y. Chen., “Fe₃O₄/Polypyrrole/Au nanocomposites with core/shell/shell structure: synthesis, characterization, and their electrochemical properties”, *Langmuir*, vol. 24, pp. 13748-13752, (2008).
16. M. Fang., V. Strom., R. T. Olsson., L. Belova., K. V. Rao., “Particle size and magnetic properties dependence on growth temperature for rapid mixed co-precipitated magnetite nanoparticles”, *Nanotech.*, vol. 23, pp. 145601, (2012).
17. W. Wu., X. Xiao., S. Zhang., J. Zhou., L. Fan., F. Ren., C. Jiang., “Large-Scale and Controlled Synthesis of Iron Oxide Magnetic Short Nanotubes: Shape Evolution, Growth Mechanism, and Magnetic Properties”, *J. Phys. Chem. C*, vol. 114, pp. 16092-16103, (2010).
18. T. Iwasaki.,S. N. Nami.,K. Kosaka., S. Watano., T. Yanagida., T. Kawai., “Direct transformation from goethite to magnetite nanoparticles by mechanochemical reduction”, *J. Alloy. Compd.*, vol. 509(4), pp. L34–L37, (2011).
19. G. Vaidyanathan., S. Sendhilnathan., R. Arulmurugan., “Structural and magnetic properties of Co_{1-x}Zn_xFe₂O₄ nanoparticles by co-precipitation method,” *J. Magn. Magn. Mater.*, vol. 313, pp. 293 – 299, (2007).
20. L. Li., X. L. Liu., M. Gao., W. Hong., G. Z. Liu., L. Liu., G. W. Song., and Z. S. Xu., “The adsorption on magnetic hybrid Fe₃O₄/HKUST-1/GO of methylene blue from water solution,” *Journal of Materials Chemistry A*, , vol. 2, pp. 1795, (2014).
21. R. I. Masel, *Principles of adsorption and reaction on solid surfaces*, John Wiley & Sons, (1996).